Peculiar electronic states, symmetries, and Berry phases in irradiated α-T_{3} materials

Andrii Iurov, Godfrey Gumbs, and Danhong Huang

Phys. Rev. B **99**, 205135 — Published 20 May 2019

DOI: 10.1103/PhysRevB.99.205135

Peculiar electronic states, symmetries and Berry phases in irradiated α-T_3 materials

Andrii Iurov[1]*, Godfrey Gumbs[2,3], and Danhong Huang[4,1]
[1] *Center for High Technology Materials, University of New Mexico, 1313 Goddard SE, Albuquerque, New Mexico, 87106, USA*
[2] *Department of Physics and Astronomy, Hunter College of the City University of New York, 695 Park Avenue, New York, New York 10065, USA*
[3] *Donostia International Physics Center (DIPC), P de Manuel Lardizabal, 4, 20018 San Sebastian, Basque Country, Spain*
[4] *Air Force Research Laboratory, Space Vehicles Directorate, Kirtland Air Force Base, New Mexico 87117, USA*
(Dated: May 3, 2019)

We have laid out the results of a rigorous theoretical investigation into the response of electron dressed states, i.e., interacting Floquet states arising from the off-resonant coupling of Dirac pseudospin-1 electrons in α-T_3 lattices, to external radiation with various polarizations. Specifically, we have examined the role played by the hopping-scale parameter α that is a measure of the coupling strength with an additional atom at the center of the honeycomb graphene lattice and which, when varied, continuously gives rise to different Berry phases. We have found that the electronic properties of the α -T_3 model (consisting of a flat band and two cones) could be significantly modified depending on the polarization of the imposed irradiation. We have demonstrated that under elliptically polarized light the low-energy band structure of such lattices will directly depend on the valley index. We have obtained and analyzed the wave functions, their symmetries and the corresponding Berry phases, connections and curvatures, and revealed that such field-modified geometry phases could be finite even for a dice lattice, which has not been observed in the absence of an optical dressing field. These results lead to possible radiation-induced band structure control and engineering, as well as experimental and technological realization of such optoelectronic and integrated photonic devices.

PACS numbers: 03.65.Vf, 73.90.+f, 73.43.Cd, 42.50.Ct

I. INTRODUCTION

The α-T_3 model is considered to be the most recent and promising member of novel two-dimensional (2D) materials. Their low-energy dispersions are obtained from a pseudospin-1 Dirac-Weyl Hamiltonian [1,2] and possess a strong similarity in comparison with graphene. [3–5] The atomic structure of the α-T_3 model is represented by a honeycomb lattice with an additional site at the center (a hub atom) of each hexagon. The model Hamiltonian depends on a hopping-scale parameter $\alpha = \tan\phi$ which is a measure of the coupling strength with the hub atom and depends on the ratio of the two hopping coefficients for all hub-rim and rim-to-rim sites. Both α and ϕ may be varied continuously and the Berry phase could be expressed in terms of these two parameters and play a crucial role in controlling many of the electronic and many-body properties of such 2D lattice structures.

The most encouraging technological opportunity for α-T_3 is its applicability for tuning the value of the parameter α from 0 to 1. The results for graphene correspond to the $\alpha \to 0$ limit of this model, while the $\alpha \to 1$ limit is connected to a class of available pseudospin-1 materials. [1,6,7] Such unique tunability together with associated electron-state evolutions have made studying various properties of these α-T_3 materials as one of the most desirable directions in present-day condensed-matter physics, chemistry and technology.

One of the latest advances in laser and microwave technologies has resulted in the possibility of an efficient control, as well as tunability of the basic electronic properties, low-energy band structures including bandgap and corresponding spin- and valley-dependent electronic states by applying an off-resonant periodic field. Electron states generated in such a way are referred to as either *electron* (or *optical*) *dressed states* and represent a single quantum object of strongly coupled light and matter. These dressed states are further characterized by different polarizations of an imposed field, as schematically displayed in Fig. 1. The effect of such light-matter interaction on modifying key electronic properties could vary substantially, depending on the type of polarizations of incoming radiation. Most of the important characteristics of such dressed states could be deduced from conventional Floquet theory, which effectively describes an extremely wide range of quantum-mechanical systems under an external periodic field. [8–11] Based

* E-mail contact: aiurov@unm.edu, theorist.physics@gmail.com

on these theories, researchers have proposed and developed numerous techniques to modify the existing electronic properties of condensed-matter materials, which was subsequently referred to as "Floquet engineering" of various nanostructures [12–14] and especially for the novel low-dimensional Dirac-cone materials. [15–22] Considerable effort has been devoted to find a way to present topological-insulator properties in such systems under irradiation. [12,23,24] Optical dressing can also alter the tunneling and conductance [25] properties of a topological insulator, leading to tunable spin transport on their surfaces [26] or edges with potential applications in spintronics, and resulting in an optically-stimulated Lifshitz transition as well. [27]

Another important property of such electronic dressed systems for operating an optoelectronic device is the challenge of confining these electron states within a specific spatial region. This is directly related to the presence or absence of the so-called Klein paradox [28] in α-T_3 materials. Circularly polarized radiation is known to open an energy gap in initially metallic graphene, [15,29] leading to a suppression of either electron transmission [30,31] or electronic trapping [32] experimentally. For systems with a band gap, such as buckled honeycomb lattices, the modification of this energy gap depends on its initial value and could be either increased or decreased, [16] which can affect all collective electronic properties in a nontrivial way. [33] In contrast, radiation with a linear polarization does not generate any band gaps, but can lead to a strong anisotropy in energy dispersions of α-T_3 material.[34] Here, we would like to emphasize that the right term in referring to the Floquet quasiparticles is the *quasienergy*. Even though sometimes we still use the word "energy" meaning the eigenvalues of a Hamiltonian equation, the distinction is crucial and should be always recognized. For such anisotropic massless fermions, a full head-on transmission is replaced by asymmetric Klein tunneling [35] with an important advance in electron technologies, i.e., electron confinement in a 2D material. Interestingly, such unique Klein tunneling within α-T_3 materials [36] with $\alpha < 1$ has been shown to be different from both graphene ($\alpha = 0$) and dice lattice ($\alpha = 1$). [37]

The principal focus of the present work is to develop a formalism for investigating the properties of optical dressed states for the α-T_3 model corresponding to well-known polarizations of incoming radiation, i.e., elliptical (and circular as a special case) and linear. From a physics point of view, elliptically polarized light has the combined effect of opening two generally inequivalent band gaps, just as it was shown for circularly polarized light. It also induces an in-plane anisotropy, related to linear polarization. Therefore, one can use elliptically polarized fields for tuning and control of these optically induced modifications of the electronic states. Contrary to recent work, [2] we concentrate on deriving closed-form analytic approximations and the wave-vector dependence of the energy dispersions around each valley, determine and analyze the corresponding wave functions, their symmetries, and the corresponding Berry phases which are now significantly modified by electron-light coupling.

We have conducted a comprehensive investigation of the way in which the Berry phase of α-T_3 is modified in the presence of irradiation. The procedure is significantly different from the study of the properties of dressed states for various phases ϕ. These phases are not equivalent to the Berry phases, even though they are directly and uniquely related. We have found that the dice lattice could acquire a finite Berry phase due specifically to the irradiation, while it was zero initially. Generally, the Berry phases substantially depend on the material parameter α and the electron-light coupling λ_0, as well as the polarization of the dressing field. The Berry phase was proven to be connected to most physical properties of α-T_3 lattices. [38] Researchers have found that its orbital susceptibility will undergo a transition from diamagnetic in graphene to paramagnetic in a dice material, [10,39] which was also demonstrated by using a tight-binding model. [40] The same conclusion applies to magneto-transport in α-T_3 materials, [41] where the calculated conductivities present several peaks, and each of these peaks will be split if α is finite. [42,43] Therefore, one of our goals in this paper aims at studying how the geometric Berry phase of α-T_3 lattices is modified in the presence of an optical dressing field.

Our results can be verified by experimental measurements, such as STM, [44] TEM, [45] angle resolved photoemission spectroscopy (ARPES) and scanning tunneling spectroscopy (STS) applications. [46] Recently, the Floquet states, their topological properties and even the Berry curvatures have received a great deal of attention by experimentalists, including Refs. [47,48].

The rest of this paper is organized in the following way. In Sec. II, we provide a brief description of important electronic properties, including low-energy band structures in the vicinity of the K and K' valleys, their corresponding wave functions, and revealing all their dependences on the geometry phase parameter $\phi(\alpha)$ as well. Following this, we present our detailed derivations for off-resonance electron Floquet states under elliptically, circularly and linearly polarized irradiation. Meanwhile, we also show corresponding eigenstates for such dressed electrons and analyze their structure and symmetry properties. Specifically, we examine how all our results depend on $\phi(\alpha)$ and on electron-field coupling λ_0. We also indicate some cases in which the band structures become valley dependent. In Sec. III, we calculate Berry phases for different eigenstates, provide analytical expressions for them, and discuss their properties. Our concluding remarks are provided in Sec. IV. In addition, detailed derivations of all our major results are given in Appendices A, B and C.

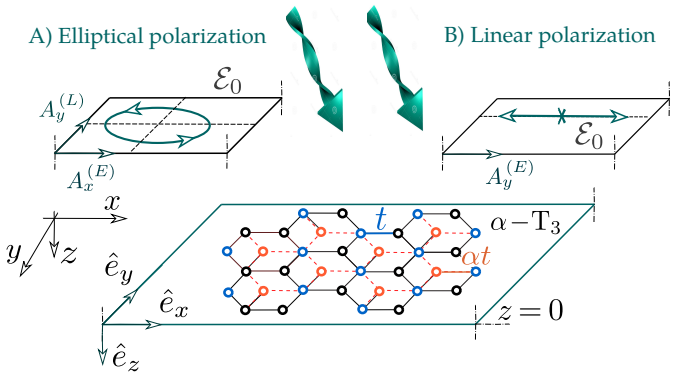

FIG. 1: Schematics of an α-T_3 lattice (in xy-plane) irradiated with A) elliptically and B) linearly polarized off-resonance optical dressing field. In each case, $\mathcal{E}_0$ represents the amplitude of the electric-field component of incident light.

II. ELECTRON DRESSED STATES

In this section, our goal is to obtain quasienergy dispersions and wave functions of quasiparticle dressed states by incident light with elliptical, circular and linear polarizations. In calculating these quantities, we are mainly concerned with elucidating the effect of Berry phase ϕ on these dressed states.

To establish notations, we start with an overview of the low-energy Hamiltonian of the α-T_3 model, its eigenfunctions and energy dispersions. The eigenstates are determined from the following ϕ-dependent pseudospin-1 Dirac-Weyl Hamiltonian [2]

$$\hat{\mathbb{H}}_\tau^\phi(\boldsymbol{k}) = \hbar v_F \begin{bmatrix} 0 & k_-^\tau \cos\phi & 0 \\ k_+^\tau \cos\phi & 0 & k_-^\tau \sin\phi \\ 0 & k_+^\tau \sin\phi & 0 \end{bmatrix}, \tag{1}$$

where $\boldsymbol{k} = (k_x, k_y)$ is a 2D wave-vector, $k_\pm^\tau = \tau k_x \pm i k_y$ with $\tau = \pm$ labeling two different valleys and v_F denoting the Fermi velocity. In Eq. (1), $\alpha = \tan\phi$ is a bonding-strength parameter in Fig. 1, characterizing an α-T_3 lattice. For $\alpha = 1$ or $\phi = \pi/4$, this Hamiltonian reduces to that of a dice lattice [1]. Three energy bands of the Hamiltonian in Eq. (1) are $E_\gamma^{(0)}(\boldsymbol{k}) = \gamma\,\hbar v_F k$, corresponding to valence ($\gamma = -1$), conduction ($\gamma = +1$) and flat ($\gamma = 0$) bands of electrons. These energy bands are degenerate with respect to τ and ϕ. Their corresponding wave functions are

$$\Psi_0^{\gamma=\pm1}(\boldsymbol{k}|\,\tau,\phi) = \frac{1}{\sqrt{2}} \begin{Bmatrix} \tau\cos\phi\ \mathrm{e}^{-i\tau\theta_{\mathbf{k}}} \\ \gamma \\ \tau\sin\phi\ \mathrm{e}^{i\tau\theta_{\mathbf{k}}} \end{Bmatrix}, \tag{2}$$

where $\theta_{\mathbf{k}} = \arctan(k_y/k_x)$ is the angle associated with the wave-vector $\boldsymbol{k}$, and

$$\Psi_0^{\gamma=0}(\boldsymbol{k}|\,\tau,\phi) = \begin{Bmatrix} \tau\sin\phi\ \mathrm{e}^{-i\tau\theta_{\mathbf{k}}} \\ 0 \\ -\tau\cos\phi\ \mathrm{e}^{i\tau\theta_{\mathbf{k}}} \end{Bmatrix}. \tag{3}$$

Unlike the degenerate electron dispersions $E_\gamma^{(0)}(\boldsymbol{k})$, the energy dispersion of dressed-state quasiparticles depends on the Berry phase ϕ and valley τ.

A. Elliptically polarized radiation

The vector potential for elliptically polarized light will depend on the direction of the major axis of the polarization ellipse. By assuming that this major axis is collinear with the x-axis, the expression for such a vector potential takes the form [16]

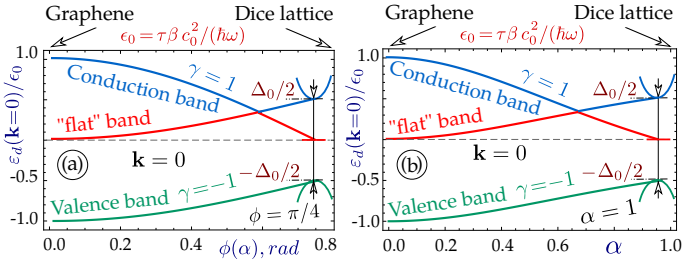

FIG. 2: Bandedges $\varepsilon_d^{(e)}(\boldsymbol{k}=0|\,\tau,\phi)$ (at either K or K' point depending on valley index $\tau=\pm1$) calculated from Eqs. (11) and (12) for dressed states in α-T_3 lattices under elliptically polarized light as a function of $\phi=\arctan(\alpha)$ in (a) and α in (b). In each panel, the conduction, valence and "flat" band dispersions correspond to blue, green and red curves, respectively. As usual, the bandgap is still defined as the energy separation between the valence and conduction bands. Here, the upper conduction band touches the middle "flat" band in both panels and $\epsilon_0=\tau\beta\, c_0^2/\hbar\omega$ is the unit for energy bands.

$$\boldsymbol{A}^{(e)}(t)=\begin{bmatrix}A_x^{(e)}(t)\\ A_y^{(e)}(t)\end{bmatrix}=\frac{\mathcal{E}_0}{\omega}\begin{bmatrix}\cos(\omega t)\\ \beta\sin(\omega t)\end{bmatrix}\,, \tag{4}$$

where the superscript "(e)" stands for elliptical polarization, $\beta=\sin\Theta_e\neq1$ is the ratio of field strengths along the two axes of the polarization ellipse. Equation (4) represents the most general form of various polarization types, where $\beta\to1$ corresponds to circularly polarized light with equal but $\pi/2$ phase-shifted components, and $\beta\to0$ describes linearly polarized radiation, given by Eq. (23).

It is important to mention that as in previous studies [34] of graphene, the dressed-state energy dispersions obtained with a semiclassical time-dependent representation as in Eq. (4) are found equivalent to that [15] derived from a quantum-field theory in the limit of a large occupation number of photons.

By making use of the canonical substitution, $k_{x,y}\to k_{x,y}-(e/\hbar)\,A_{x,y}^{(e)}(t)$, the field-free Hamiltonian in Eq. (1) is changed into

$$\hat{\mathbb{H}}_\tau^\phi(\boldsymbol{k})\Longrightarrow\hat{\mathcal{H}}^{(e)}(\boldsymbol{k},t|\,\tau,\phi)\equiv\hat{\mathbb{H}}_\tau^\phi(\boldsymbol{k})+\hat{\mathbb{H}}_A^{(e)}(t|\,\tau,\phi)\,, \tag{5}$$

where the interaction term is given by

$$\hat{\mathbb{H}}_A^{(e)}(t|\,\tau,\phi)=-\tau c_0\left\{\begin{bmatrix}0 & \mathsf{e}^{-i\tau\Omega_\beta(t)}\cos\phi & 0\\ 0 & 0 & \mathsf{e}^{-i\tau\Omega_\beta(t)}\sin\phi\\ 0 & 0 & 0\end{bmatrix}+\ h.c.\right\}\,. \tag{6}$$

In Eq. (6), $h.c.$ represents the Hermitian conjugate of the preceding matrix and $\Omega_\beta(t)=\arctan\left[\beta\tan(\omega t)\right]$ turns into (ωt) for circularly polarized light. The interaction strength, $c_0=e\mathcal{E}_0v_F/\omega$, is the same for linearly polarized light. Apart from c_0, we also introduce another dimensionless coupling constant $\lambda_0=c_0/\hbar\omega$ in our calculations. Since our studies aim at an off-resonant high-frequency irradiation with $E_\gamma^{(0)}(\boldsymbol{k})/\hbar\omega\ll1$, we can treat λ_0 as a small parameter,[64] and therefore corresponding series expansions could be executed with it.

If the field-free Hamiltonian is linear in k, which holds true for nearly all Dirac and gapped Dirac structures, e.g., gapped or gapless graphene, buckled honeycomb lattices and transition metal dichalcogenides, the corresponding Hamiltonian for dressed states can be obtained simply by adding a single $\boldsymbol{k}$-interaction term. However, the situation becomes drastically different for phosphorene with a more complicated anisotropic $\boldsymbol{k}$ dependence in its field-free Hamiltonian. [17]

Mathematically, in order to solve the current eigenvalue problem, we have to rely on a *perturbation theory*. Moreover, nearly all off-resonant systems, subjected to an external periodic field with $E_\gamma^{(0)}(\boldsymbol{k})\ll\hbar\omega$, could be effectively described by a perturbative Floquet-Magnus expansion [8] of the interaction Hamiltonian in powers of $(1/\hbar\omega)$. Eventually, this allows for an approximate solution whenever the exact diagonalization of an interaction matrix becomes impossible, [16] or at least it substantially simplifies a very lengthy calculation. [17]

The key idea for using the perturbation approach is the following. Once the interaction Hamiltonian term $\mathbb{H}_A^{(e)}(t|\,\tau,\phi)$ is expressed as

$$\hat{\mathbb{H}}_A^{(e)}(t|\,\tau,\phi) = \hat{\mathbb{P}}_{\tau,\phi}\,\mathsf{e}^{i\omega t} + \hat{\mathbb{P}}^{\dagger}_{\tau,\phi}\,\mathsf{e}^{-i\omega t}\,, \tag{7}$$

where the operator $\hat{\mathbb{P}}_{\tau,\phi}$ and its Hermitian conjugate $\hat{\mathbb{P}}^{\dagger}_{\tau,\phi}$ are *time-independent*, the effective Hamiltonian representing our dressed-state system becomes [8]

$$\hat{\mathcal{H}}_{\rm eff}^{(e)}(\boldsymbol{k},t|\,\tau,\phi) = \hat{\mathbb{H}}_{\tau}^{\phi}(\boldsymbol{k}) + \frac{1}{\hbar\omega}\left[\hat{\mathbb{P}}_{\tau,\phi},\,\hat{\mathbb{P}}^{\dagger}_{\tau,\phi}\right]_{-} + \frac{1}{2(\hbar\omega)^2}\left\{\left[\left[\hat{\mathbb{P}}_{\tau,\phi},\,\hat{\mathbb{H}}_{\tau}^{\phi}(\boldsymbol{k})\right]_{-},\,\hat{\mathbb{P}}^{\dagger}_{\tau,\phi}\right]_{-} + \,h.c.\right\} + \cdots \quad , \tag{8}$$

where $[\hat{A},\hat{B}]_{-} \equiv \hat{A}\hat{B} - \hat{B}\hat{A}$.

For most situations, it is sufficient to retain the first two terms of such a power series in Eq. (8). In our case, combining with Eqs. (6) and (7) we obtain explicitly the time-independent perturbation operator $\hat{\mathbb{P}}_{\tau,\phi}$ as

$$\hat{\mathbb{P}}_{\tau,\phi} = -\frac{c_0}{2}\begin{bmatrix} 0 & (\tau-\beta)\cos\phi & 0 \\ (\tau+\beta)\cos\phi & 0 & (\tau-\beta)\sin\phi \\ 0 & (\tau+\beta)\sin\phi & 0 \end{bmatrix}\,. \tag{9}$$

This matrix is real, but clearly not Hermitian, as it always occurs for all types of circularly polarized radiation, including the general elliptical polarization with $0 \le \beta < 1$.

After evaluating the commutation relation in Eq. (8), we arrive at the following expression for the effective perturbation Hamiltonian up to the order of $\mathcal{O}(\lambda_0^2)$

$$\hat{\mathcal{H}}_{\rm eff}^{(e)}(\boldsymbol{k}|\,\tau,\phi) = \hat{\mathbb{H}}_{\tau}^{\phi}(\boldsymbol{k}) - \tau\beta\lambda_0 c_0\begin{bmatrix} \cos^2\phi & 0 & 0 \\ 0 & -\cos(2\phi) & 0 \\ 0 & 0 & -\sin^2\phi \end{bmatrix} - \frac{\tau}{4}\,\hbar v_F\lambda_0^2\begin{bmatrix} 0 & h_{12}(\boldsymbol{k}|\,\tau,\phi) & 0 \\ h_{12}^{*}(\boldsymbol{k}|\,\tau,\phi) & 0 & h_{23}(\boldsymbol{k}|\,\tau,\phi) \\ 0 & h_{23}^{*}(\boldsymbol{k}|\,\tau,\phi) & 0 \end{bmatrix}\,, \tag{10}$$

where $h_{12}(\boldsymbol{k}|\,\tau,\phi) = \cos\phi\,[1+3\cos(2\phi)]\,(\beta^2 k_x - i\tau k_y)$ and $h_{23}(\boldsymbol{k}|\,\tau,\phi) = \sin\phi\,[1-3\cos(2\phi)]\,(\beta^2 k_x - i\tau k_y)$.

It is important to point out that the chirality $k_{\pm}^{\tau} \equiv \tau k_x \pm i k_y$ kept in the third term of Eq. (10) for $\beta = 1$ is the same as that in $\hat{\mathbb{H}}_{\tau}^{\phi}(\boldsymbol{k})$ given by Eq. (1). It is also interesting to check the second term of Eq. (10), which is independent of $\boldsymbol{k}$ and determines the dressed-state bandedges $\varepsilon_d^{(e)}(\boldsymbol{k}=0|\,\tau,\phi)$ at the K point, i.e.,

$$\varepsilon_d^{(e)}(\boldsymbol{k}=0|\,\tau,\phi) = \tau\beta\frac{c_0^2}{\hbar\omega}\,\times\begin{cases} -\cos^2\phi \\ +\cos(2\phi) \\ +\sin^2\phi \end{cases} = \tau\beta\lambda_0 c_0\,\times\begin{cases} -1/\left(1+\alpha^2\right) \\ \left(1-\alpha^2\right)/\left(1+\alpha^2\right) \\ \alpha^2/\left(1+\alpha^2\right) \end{cases}\,, \tag{11}$$

as well as the energy gap $\delta_0(\phi)$ between the valence and conduction bands

$$\delta_0(\phi) = \frac{\beta}{2}\,\lambda_0 c_0\,\times\begin{cases} \cos(2\phi)+\cos^2\phi\,, & \text{for}\;\; 0 \le \phi < \phi_0 \\ 1\,, & \text{for}\;\; \phi_0 < \phi \le \pi/4\,, \end{cases} \tag{12}$$

where $\phi_0 = 0.615\,rad \backsimeq 0.196\,\pi$ or $\alpha_0 = 1/\sqrt{2}$ and the subscript "d" stands for dressed states. Hereafter, we will omit the λ_0 dependence in other expressions for simplicity.

The simple but important bandedge and bandgap results in Eqs. (11) and (12) can be seen in Fig. 2. Each energy is given in units of $\epsilon_0 = \tau\beta\,c_0^2/\hbar\omega$, i.e., its actual value depends on the valley index τ, the ratio of the ellipse polarization axes β, the electron-light interaction strength c_0, and the dimensionless coupling constant λ_0. The "flat" band is actually not flat anymore, and all three bands are now distorted and intersect with each other. Even for $\beta = 1$, the energy bandgap changes from $\lambda_0 c_0$ for graphene to $\lambda_0 c_0/2$ for a dice lattice. It is intriguing to find that the bandgap remains as a constant in the region of $\phi > \phi_0$ or $\alpha > \alpha_0$. The bandgap of a dice lattice is the smallest and exactly half

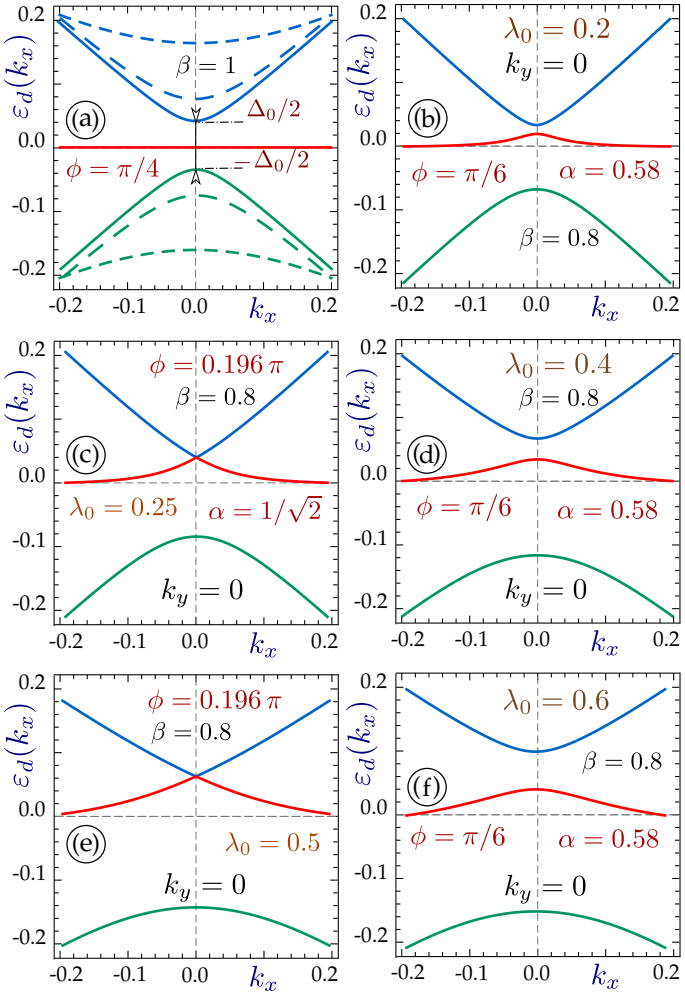

FIG. 3: Numerically calculated dressed-state energy dispersions $\varepsilon_d^{(e)}(\boldsymbol{k}|\,\tau,\phi)$ based on Eq. (10) under elliptically polarized and off-resonant irradiation with $\beta = 0.8$ as functions of k_x for $k_y = 0$. All results are obtained in the vicinity of the K valley with $\tau = 1$. Each plot involves dispersions for three bands, i.e., conduction ($\gamma = 1$, blue), valence ($\gamma = -1$, green) and "flat" ($\gamma = 0$, red) bands. Here, panel (a) presents results for a dice lattice ($\phi = \pi/4$) under circularly polarized irradiation ($\beta = 1$) with $\lambda_0 = 0.2$ (solid), 0.4 (long-dashed) and 0.6 (short-dashed). Plots (c), (e) on the left correspond to Berry phase $\phi = 0.196\,\pi$ with $\lambda_0 = 0.25$ in (c) and $\lambda_0 = 0.5$ in (e), having closed bandgap between the conduction and "flat" bands. Panels (b), (d), (f) on the right are for $\phi = \pi/6$ at $\lambda_0 = 0.2$ (b), 0.4 (d) and 0.6 (f). Here, the unit for energy bands is ϵ_0.

of that for graphene (the largest). The α-dependence of the bandedge locations, presented in Fig. 2(b) for comparison, is similar but not exactly identical to the corresponding dependence on ϕ. Although analytical solutions for band dispersions at finite k could be obtained from a third-power algebraic equation, the expressions are too lengthy to be shown and analyzed.

Our numerical results for the energy dispersions $\varepsilon_d^{(e)}(\boldsymbol{k}|\,\tau,\phi)$ for the elliptically polarized light are presented in Fig. 3. Besides the simplest case with $\phi = \pi/4$, which was discussed above and presented in Fig. 3(a), we examine the remaining ones and find that the initially flat band $E_0^{(0)}(\boldsymbol{k}) \equiv 0$ acquires a $\boldsymbol{k}$-dependent non-zero curvature and can sit either above or below the zero line depending on the selection of Berry phase ϕ as well as the valley index τ (not shown). The valence and conduction bandedges are shifted individually in energies, and therefore we see no mirror symmetry with respect to the zero line between valence and conduction bands, as was noticed in Ref. [2]. However, a complete inversion symmetry for $\boldsymbol{k} \to -\boldsymbol{k}$ is still kept, which implies that only even powers of wave-vector components k_x and k_y will appear in the eigenvalue equation associated with the Hamiltonian $\hat{\mathcal{H}}_{\rm eff}^{(e)}(\boldsymbol{k}, t|\,\tau,\phi)$ in Eq. (10). Apparently, the effect from the imposed radiation on the flat band and its distortion around the zero line become most visible near $\boldsymbol{k} = 0$. We would like to emphasize that such distortion behavior and β dependence in these dispersions result from the anisotropy of incident light and are absent for circularly polarized radiation with $\beta = 1$.

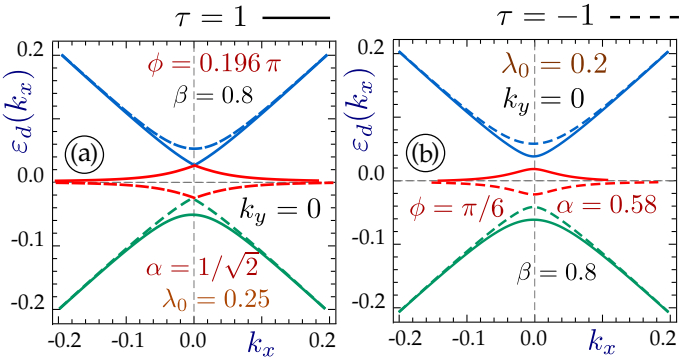

FIG. 4: Numerically calculated valley-dependent dressed-state quasienergies $\varepsilon_d^{(e)}(\boldsymbol{k}|\,\tau,\phi)$ based on Eq. (10) under an elliptically polarized dressing field with $\beta = 0.8$. We plot $\varepsilon_d^{(e)}(\boldsymbol{k}|\,\tau,\phi)$ as functions of k_x for $k_y = 0$. Panel (a) presents dispersions for $\phi = 0.196\,\pi$, while panel (b) shows plots for $\phi = \pi/6$. In each plot, $\lambda_0 = 0.25$, where solid curves correspond to K valley with $\tau = 1$, whereas dashed ones to K' with $\tau = -1$. Here, the "flat" band touches either the conduction or the valence band in panel (a) for $\tau = 1$ and $\tau = -1$, respectively, and the unit for energy bands is ϵ_0.

Actually, not just the band edges and gaps from Eqs. (11) and (12), but the whole $\boldsymbol{k}$ dispersions of energy bands in Fig. 4 demonstrate their direct and substantial dependence on valley index $\tau = \pm 1$. Here, the location of each energy band varies near the K and K' valleys, and this noticeable difference is certainly not limited to just a sign switching, in contrast to all situations studied before. As $\phi = 0.196\,\pi$ or $\alpha = 1/\sqrt{2}$, either upper or lower bandgap is closed, depending on τ value. Consequently, we expect non-equivalent density of electronic states in each low-energy (near K or K') region. The contributions from these τ-dependent density of electronic states will not be equal or simply opposite to each other, leading directly to valley-dependent optical and transport properties.

The $\varepsilon_d^{(e)}(\boldsymbol{k}|\,\tau,\phi)$ dispersions also display a striking resemblance to silicene, in which the electronic states with a given spin $\sigma = \pm 1$ present two inequivalent band gaps $\Delta_{\tau,\sigma} = |\Delta_{\rm SO} - \sigma\tau\Delta_z|$, in which $\Delta_{\rm SO}$ is a constant intrinsic spin-orbit gap and Δ_z can be tuned continuously by an external perpendicular electrostatic field. Therefore, by varying the field strength, one of the gaps between the conduction and valence bands can be either opened or closed, and then such a buckled honeycomb lattice would behave like a topological insulator, valley-spin polarized metal or just a conventional band insulator. Here, the lower energy gap $|\Delta_{SO} - \Delta_z|$, which defines a physical band gap between the valence and conduction bands, changes into the upper one $\Delta_{SO} + \Delta_z$ as either the valley index τ or the spin index σ switches its sign. [49,50] This unique dependence gives rise to specific transport properties [51] and many valleytronics applications [52], and more importantly it could be realized by α-T_3 lattice under elliptically polarized irradiation.

As a comparison, for graphene with $E_\gamma^{(0)}(|\boldsymbol{k}|) = \gamma\hbar v_F|\boldsymbol{k}|$ and interacting with circularly polarized radiation, we find the dispersion relation for off-resonant dressed states can be expressed as

$$\varepsilon_d^{\gamma}(\boldsymbol{k}) = \gamma\sqrt{\left(\frac{c_0^2}{\hbar\omega}\right)^2 + \left\{\hbar v_F k\left[1 - 2\left(\frac{c_0}{\hbar\omega}\right)^2\right]\right\}^2}\,, \tag{13}$$

which could be derived from the limit of vanishing anisotropy for multilayer black phosphorus [17] or by setting all band gaps to zero for transition metal dichalcogenides [16]. The explicit expression in Eq. (13) is a result of expansion up to the order of $\mathcal{O}[1/(\hbar\omega)^2]$. On the other hand, an exact solution predicts [15] that the energy band gap is given by

$$2\delta_d = \sqrt{(\hbar\omega)^2 + 4c_0^2} - \hbar\omega \backsimeq \frac{2c_0^2}{\hbar\omega}\left[1 - \left(\frac{c_0}{\hbar\omega}\right)^2 + \cdots\right]\,. \tag{14}$$

Consequently, from Eq. (12) we know the field-induced energy bandgap in Eq. (14) for graphene is exactly twice as large as that of a dice lattice (taking $\beta = 1$).

B. Symmetric band structure and wave function of a dice lattice

In this part, we would like to address spin-1 dice lattices with $\alpha = 1$ or $\phi = \pi/4$ as a special case, in which all the equations are greatly simplified and analytical expressions can be obtained to gain a deeper insight into dressed-

electron dynamics. It is also interesting to notice that the effect of irradiation becomes the smallest in this case for a given dressing-field intensity, as we see by comparing Fig. 3(a) with Figs. 3(b), (d), (f). Moreover, this case has its own significance in device applications since T_3 spin-1 materials could be possibly synthesized now.

In this case, the non-interacting Hamiltonian (1) for a dice lattice takes the form

$$\hat{\mathbb{H}}^{d}_{\tau}(\boldsymbol{k}|\,\tau) = \frac{\hbar v_F}{\sqrt{2}} \begin{bmatrix} 0 & k^{-}_{\tau} & 0 \\ k^{+}_{\tau} & 0 & k^{-}_{\tau} \\ 0 & k^{+}_{\tau} & 0 \end{bmatrix} = \sum_{\alpha=\pm} k^{\,\alpha}_{\tau}\, \hat{\Sigma}^{(1)}_{\alpha} \;, \tag{15}$$

where $\hat{\Sigma}^{(1)}_{\pm 1} = \hat{\Sigma}^{(1)}_{x} \pm i\hat{\Sigma}^{(1)}_{y}$ are defined based on spin-1 matrices in Appendix A. By expanding the Hamiltonian in Eq. (15) up to the order of $\mathcal{O}[1/(\hbar\omega)^2]$, the effective Hamiltonian in Eq. (10) becomes

$$\hat{\mathcal{H}}^{(e)}_{\rm eff}(\boldsymbol{k}|\,\tau) \backsimeq \begin{bmatrix} -(\tau\beta/4)\,\lambda_0 c_0 & \mathcal{G}(\boldsymbol{k}|\,\tau) & 0 \\ 0 & 0 & \mathcal{G}(\boldsymbol{k}|\,\tau) \\ 0 & 0 & (\tau\beta/4)\,\lambda_0 c_0 \end{bmatrix} + \; h.c. \;, \tag{16}$$

where

$$\mathcal{G}(\boldsymbol{k}|\,\tau) = \frac{\hbar v_F}{\sqrt{2}} \left[\tau k_x \left(1 + \frac{\beta^2\lambda_0^2}{4}\right) - i k_y \left(1 + \frac{\lambda_0^2}{4}\right)\right] \;. \tag{17}$$

Here, the significant simplification of Eq. (10) has been made possible mainly due to the fact that $h_{12}(\boldsymbol{k}|\,\tau) = h_{23}(\boldsymbol{k}|\,\tau) = 1/\sqrt{2}\,(\beta^2 k_x - i\tau k_y)$ at $\phi = \pi/4$.

For the effective Hamiltonian in Eq. (16), the low-energy band structure is symmetric with respect to electrons and holes, given by one flat and two dispersive bands

$$\begin{aligned} &\varepsilon^{(e)}_{d}(\boldsymbol{k}) = 0 \quad \text{and} \quad \varepsilon^{(e)}_{d}(\boldsymbol{k}) = \pm\sqrt{\mathcal{S}(\boldsymbol{k})} \;, \quad \text{where} \\ &\mathcal{S}(\boldsymbol{k}) = \left(\frac{\beta\lambda_0 c_0}{4}\right)^2 + (\hbar v_F)^2 \left\{k^2 + \frac{\lambda_0^2}{2}\left[(\beta k_x)^2\left(1 + \frac{\beta^2\lambda_0^2}{8}\right) + k_y^2\left(1 + \frac{\lambda_0^2}{8}\right)\right]\right\} \;, \end{aligned} \tag{18}$$

which becomes independent of valley index τ. Only in this case do the middle band stay flat for all wave-vectors $\boldsymbol{k}$, while the dispersive valence and conduction bands remain symmetric to $\gamma = \pm 1$ at the same time. From Eq. (18) we know the opening of a finite bandgap in this case is the same as $\delta_0 = \beta\lambda_0 c_0/2$ given by Eq. (12) at $\phi = \pi/4$. It is clear that the anisotropy of the energy bands comes solely from the elliptical polarization of the dressing field and disappears for $\beta = 1$. From now on, we will focus only on the latter case for circularly polarized radiation. In this way, the energy index $\gamma = \pm 1$ still labels a Dirac cone with a *renormalized isotropic* Fermi velocity $\bar{v}_F = v_F\,\left(1 + \lambda_0^2/4\right)$.

Now we can find the wave functions for disersions (18). The solutions, pertaining to the valence and conduction bands $\gamma = \pm 1$ are

$$\Psi^{\,(E)}_{d}(\gamma, \tau\,|\,\lambda_0, \mathbf{k}) = \frac{1}{\sqrt{\mathcal{N}^{\,(\gamma)}}} \begin{Bmatrix} \tau\,\mathcal{C}^{\,(1)}\,\mathsf{e}^{-i\tau\theta_{\mathbf{k}}} \\ \mathcal{C}^{\,(2)} \\ \tau\,(\hbar v_F k)^2\,\mathsf{e}^{+i\tau\theta_{\mathbf{k}}} \end{Bmatrix} , \tag{19}$$

where

$$\begin{aligned} &\mathcal{C}^{\,(1)}(\gamma, \tau\,|\,\lambda_0, k) = (\hbar v_F k)^2 + 2\left[\Delta^2_{(\lambda)} - 2c_0\lambda_0\,\gamma\,\tau\,\sqrt{(\hbar v_F k)^2 + \Delta^2_{(\lambda)}}\right] \;, \\ &\mathcal{C}^{\,(2)}(\gamma, \tau\,|\,\lambda_0, k) = \sqrt{2}\,\gamma\,(\hbar v_F k)\,\left[\sqrt{(\hbar v_F k)^2 + \Delta^2_{(\lambda)}} - \gamma\,\tau\,\Delta_{\,(\lambda)}\right] \;, \\ &\mathcal{N}^{\,(\gamma)}(\tau\,|\,\lambda_0 \ll 1, k) \backsimeq 2\left\{2\,(\hbar v_F k)^4 - 5\gamma\,\tau\,c_0\lambda_0(\hbar v_F k)^3 + 9\,[c_0\lambda_0\,(\hbar v_F k)]^2\right\} \;. \end{aligned} \tag{20}$$

Parameter $\Delta_{\,(\lambda)} = 2\lambda_0\,c_0/(4 + \lambda_0^2)$ is not equivalent to the actual energy bandgap $2\Delta_0(\beta = 1, \lambda_0) = \lambda_0 c_0$.

For the flat band, we obtain

$$\Psi_d^{(E)}(\gamma=0,\tau\,|\,\lambda_0,\mathbf{k})=\frac{1}{\sqrt{\mathcal{N}^{(0)}}}\left\{\begin{array}{c} k\mathsf{e}^{-i\tau\theta_{\mathbf{k}}} \\ 2\sqrt{2}\,\lambda_0\,(4-\lambda_0^2)\,c_0/(\hbar v_F) \\ k\mathsf{e}^{+i\tau\theta_{\mathbf{k}}}\end{array}\right\}, \tag{21}$$

where

$$\mathcal{N}^{(0)}(\lambda_0\ll 1,k)\backsimeq 2\left[k^2+\left(8\lambda_0\,\frac{c_0}{\hbar v_F}\right)^2\right]+\ldots. \tag{22}$$

Here, the middle component of wavefunction (21) is non-zero only in the presence of circularly polarized irradiation. One can easily verify that the wave functions (19) and (21) in the limit of vanishing electron-light interaction $\lambda_0\to 0$ agree with the results in Eqs. (2) and (3).

Electronic states with a finite energy gap between the valence, "flat" and conduction bands are critical for electron confinement, gate control, as well as the investigation of *excitons* in our considered materials. The latter notion becomes extremely important, since pursuant to our results, one should now be able to construct an excitonic state and analyze their collective properties, such as Bose-Einstein condensation, [53] depending on various lattice and electron-light interaction parameters. In fact, excitons simply do not exist without a band gap, and we believe that our work indeed, for the first time, paves a new route to pursue this type of research in α-T_3.

C. Linear polarization of the incoming radiation

We now turn our attention to an alternative situation in which linearly polarized radiation will be incorporated into the α-T_3 model Hamiltonian. Being essentially anisotropic, such optical fields are known to transform the Dirac cone into an asymmetric elliptical cone without creating an energy gap between the valence and conduction bands. [34] Whereas for anisotropic phosphorene the direction of the linear polarization is important, [17] for the isotropic energy dispersions in α-T_3 lattices we can assume the field polarization lies along the x axis without loss of any generality, yielding

$$\boldsymbol{A}^{(L)}(t)=\left[\begin{array}{c} A_x^{(L)}(t) \\ 0\end{array}\right]=\frac{\mathcal{E}_0}{\omega}\left[\begin{array}{c}\cos(\omega t)\\ 0\end{array}\right]. \tag{23}$$

Assuming a linear k-dependence to the field-free Hamiltonian $\hat{\mathbb{H}}_\tau^\phi(\boldsymbol{k})$, we find the total Hamiltonian $\hat{\mathcal{H}}^{(L)}(\boldsymbol{k},t|\,\tau,\phi)$ for dressed particles only acquires an additional k-independent term, given by

$$\hat{\mathbb{H}}_\tau^\phi(\boldsymbol{k})\Longrightarrow\hat{\mathcal{H}}^{(L)}(\boldsymbol{k},t|\,\tau,\phi)=\hat{\mathbb{H}}_\tau^\phi(\boldsymbol{k})+\hat{\mathbb{H}}_A^{(L)}(t|\,\tau,\phi)\,, \tag{24}$$

where

$$\hat{\mathbb{H}}_A^{(L)}(t|\,\tau,\phi)=-\tau c_0\cos(\omega t)\left[\begin{array}{ccc}0&\cos\phi&0\\ \cos\phi&0&\sin\phi\\ 0&\sin\phi&0\end{array}\right]. \tag{25}$$

Here, the coupling constant $c_0=eE_0v_F/\omega$ is the same as that in the case of elliptically or circularly polarized light. However, each element of the matrix in Eq. (25) has the identical periodic time dependence in comparison with a circularly polarized radiation field.

The case of linearly polarized dressing field is distinguished because the time-dependent Schrődinger equation at K (or K') point for $\boldsymbol{k}=0$ *could be solved analytically*. This implies that our result regarding the absence of an energy bandgap is precise and, more importantly, wave functions with explicit time dependence could be obtained in contrast to the previous case for elliptically polarized light.

The detailed derivation of the quasienergy dispersions and the wave function for the linearly polarized dressing field is provided in Appendix B. Specifically, the τ-independent dressed-state quasiparticle energy dispersions are found as

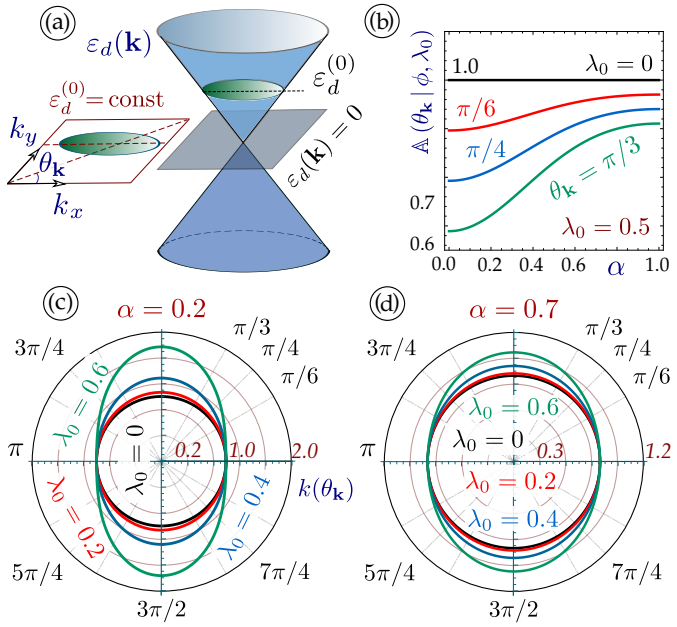

FIG. 5: (Color online) Angular dependence of the valley-independent dressed-state energy dispersions $\varepsilon^{(L)}_{d,\gamma}(\boldsymbol{k}|\,\phi)$ from Eq. (26) for the case of linearly polarized radiation applied to an α-T_3 lattice, as schematically shown in panel (a) with $\theta_{\mathbf{k}} = \arctan(k_y/k_x)$. Plot (b) demonstrates how the angular function $\mathbb{A}(\theta_{\mathbf{k}}\,|\,\phi)$, given by Eq. (27), depends on hopping-scale parameter α at various angles $\theta_{\mathbf{k}}$, where curves for $\theta_{\mathbf{k}} = \pi/6$ (red), $\pi/4$ (blue) and $\pi/3$ (green) are displayed for $\lambda_0 = 0.5$ in addition to the black line $\mathbb{A}(\theta_{\mathbf{k}}\,|\,\phi) \equiv 1$ for $\theta_{\mathbf{k}} = 0$. The two lower polar plots (c) and (d) show $\theta_{\mathbf{k}}$ dependence in Eq. (26) for fixed $\varepsilon^{(L)}_{d,\gamma}(\boldsymbol{k}|\,\phi)/E_F \equiv 0.5$, where $\lambda_0 = 0$, 0.2, 0.4, 0.6 are selected for black, red, blue, green curves.

$$\begin{aligned}
&\varepsilon^{(L)}_{d,\gamma=0}(\boldsymbol{k}|\,\phi) = 0 \ \text{ and} \\
&\varepsilon^{(L)}_{d,\gamma=\pm1}(\boldsymbol{k}|\,\phi) = \pm\hbar v_F k\,\sqrt{\mathbb{A}(\theta_{\mathbf{k}}\,|\,\phi)}
\end{aligned} \tag{26}$$

with an angular function

$$\mathbb{A}(\theta\,|\,\phi) = \cos^2\theta + \Big\{[\mathcal{J}_0(2\lambda_0)\cos(2\phi)]^2 + [\mathcal{J}_0(\lambda_0)\sin(2\phi)]^2\Big\}\,\sin^2\theta \tag{27}$$

to highlight *field-induced anisotropy*. The dispersion relations for graphene, obtained in Ref. [34], are easily recovered by setting ϕ to zero. In the opposite limit for a *dice lattice* with $\phi = \pi/4$, only the second term $\mathcal{J}_0(\lambda_0)\sin(2\phi)$ in Eq. (27) is kept, so that the effect of electron-field interaction becomes the weakest with respect to all ϕ values.

Since the off-resonant radiation with $\lambda_0 = c_0/\hbar\omega \ll 1$ is considered, the zero-order Bessel function of the first kind could be expanded up to the order of $\mathcal{O}(\lambda_0^2)$, and therefore the dispersions of conduction and valence bands in Eq. (26) are further approximated as

$$\varepsilon^{(L)}_{d,\gamma=\pm1}(\boldsymbol{k}|\,\phi) \backsimeq \pm\hbar v_F k\,\left\{1 - \frac{\lambda_0^2}{8}\,[5 + 3\cos(4\phi)]\,\sin^2\theta_{\mathbf{k}}\right\}\,. \tag{28}$$

Even for an infinitesimal coupling constant λ_0, the anisotropy, and therefore the difference in Fermi velocities along the k_x- and k_y-directions, becomes the largest for graphene ($\phi = 0$) and the smallest for a dice lattice ($\phi = \pi/4$).

Most importantly, we find the flat band $\varepsilon^{(L)}_{d,\gamma=0}(\boldsymbol{k}|\,\phi) = 0$ is not affected under linearly polarized irradiation for all wave-vectors $\boldsymbol{k}$. The valence and conduction bands, on the other hand, display anisotropy with respect to $\boldsymbol{k}$. As a result, the standard right-circular Dirac cone is transformed into an elliptic cone with its major axis parallel to the direction of incident light-field polarization. We also notice that the complete electron-hole symmetry of the upper and lower cones is preserved and there exists no energy gap between the valence and conduction bands. These

features are quite similar to corresponding results of graphene. [34] However, an important new feature comes from the ϕ-dependence in $\boldsymbol{k}$ dispersion of $\varepsilon^{(L)}_{d,\gamma=\pm1}(\boldsymbol{k}|\,\phi)$. As demonstrated in Fig. 4, the significance of induced anisotropy depends on the chosen parameter ϕ.

After a lengthy calculation as presented in Appendix B, the two wave functions, corresponding to the valence and conduction band energies with $\gamma=\pm1$ are as follows

$$\Psi^{\gamma=\pm1}_{d}(\boldsymbol{k},t|\,\tau)=\mathsf{e}^{\mp iv_Fkf_1(\theta_{\mathbf{k}})t}\,\frac{f_1(\theta_{\mathbf{k}})+\cos\theta_{\mathbf{k}}}{4f_1(\theta_{\mathbf{k}})}\left\{\mathsf{e}^{\pm iz_\lambda(t)}\begin{bmatrix}\tau\\ \pm\sqrt{2}\\ \tau\end{bmatrix}\right.$$
$$\left.-\frac{2i\,\mathcal{J}_0(\lambda_0)\sin\theta_{\mathbf{k}}}{f_1(\theta_{\mathbf{k}})+\cos\theta_{\mathbf{k}}}\begin{bmatrix}1\\0\\-1\end{bmatrix}-\left(\frac{\mathcal{J}_0(\lambda_0)\sin\theta_{\mathbf{k}}}{f_1(\theta_{\mathbf{k}})+\cos\theta_{\mathbf{k}}}\right)^2\begin{bmatrix}\tau\\ \mp\sqrt{2}\\ \tau\end{bmatrix}\mathsf{e}^{\mp iz_\lambda(t)}\right\}\,, \tag{29}$$

where

$$f_1(\theta_{\mathbf{k}})=f(\theta_{\mathbf{k}}|\,\phi=\pi/4)=\sqrt{\cos^2\theta_{\mathbf{k}}+\sin^2\theta_{\mathbf{k}}\,\mathcal{J}_0^2(\lambda_0)} \tag{30}$$

and $z_\lambda(t)=\lambda_0\sin(\omega t)$. The wave function in Eq. (29) at $t=0$ can be further simplified as

$$\Psi^{\gamma=\pm1}_{d}(\lambda_0,\boldsymbol{k})=\frac{1}{2}\begin{bmatrix}\tau\mathsf{e}^{-i\Phi_1(\theta_{\mathbf{k}}|\,\tau)}\\ \gamma\sqrt{2}\\ \tau\mathsf{e}^{i\Phi_1(\theta_{\mathbf{k}}|\,\tau)}\end{bmatrix}\,, \tag{31}$$
$$\Phi_1(\theta_{\mathbf{k}}|\,\tau)=2\arctan\left\{\tau\,\frac{\mathcal{J}_0(\lambda_0)\sin\theta_{\mathbf{k}}}{f_1(\theta_{\mathbf{k}})+\cos\theta_{\mathbf{k}}}\right\}\backsimeq\tau\left\{\theta_{\mathbf{k}}-\frac{\lambda_0^2}{8}\,\sin^2(2\theta_{\mathbf{k}})+\cdots\right\}\,.$$

The two components of the wave function in Eq. (31) are identical to each other, except for a different phase, similar to that for non-interacting dice lattice in Eq. (2) with $\phi=\pi/4$. Here, the renormalized phase $\Phi_1(\theta_{\mathbf{k}}|\,\tau)$ contains the leading-order correction proportional to the intensity of imposed radiation.

The remaining wave function for the flat band with $\gamma=0$ is given by

$$\Psi^{\gamma=0}_{d}(\boldsymbol{k},t|\,\tau)=\frac{1}{\sqrt{2}f_1(\theta_{\mathbf{k}})}\left\{-\frac{i\tau}{2}\,\sin\theta_{\mathbf{k}}\,\mathcal{J}_0(\lambda_0)\sum_{\alpha=\pm1}\mathsf{e}^{i\alpha z_\lambda(t)}\begin{bmatrix}1\\ \sqrt{2}\,\alpha\tau\\ 1\end{bmatrix}+\cos\theta_{\mathbf{k}}\begin{bmatrix}1\\0\\-1\end{bmatrix}\right\}\,. \tag{32}$$

Here, the wave function in Eq. (32) also consists of two nonzero components of equal amplitude but with a different phase $\Phi_2(\theta_{\mathbf{k}}|\,\tau)$ in comparison with Eq. (3). Similarly, the wave function in Eq. (32) at $t=0$ can be simply written as

$$\Psi^{\gamma=0}_{d}(\boldsymbol{k}|\,\tau)=\frac{1}{\sqrt{2}}\begin{bmatrix}\mathsf{e}^{-i\Phi_2(\theta_{\mathbf{k}}|\,\tau)}\\ 0\\ -\mathsf{e}^{i\Phi_2(\theta_{\mathbf{k}}|\,\tau)}\end{bmatrix}\,, \tag{33}$$
$$\Phi_2(\theta_{\mathbf{k}}|\,\tau)=\arctan\left\{\tau\mathcal{J}_0(\lambda_0)\tan\theta_{\mathbf{k}}\right\}\backsimeq\tau\left\{\theta_{\mathbf{k}}-\frac{\lambda_0^2}{2}\,\sin(2\theta_{\mathbf{k}})+\cdots\right\}\,.$$

It is interesting to compare our current results for a dice lattice with the corresponding wave function for graphene in Ref. [34]. The Dirac electron in graphene, interacting with a linearly polarized and off-resonant dressing field acquires the following energy dispersions

$$\varepsilon^{\gamma=\pm1}_{d}(\boldsymbol{k})=\gamma\hbar v_Fkf_0(\theta_{\mathbf{k}})\,, \tag{34}$$
$$f_0(\theta_{\mathbf{k}})=\sqrt{\cos^2\theta_{\mathbf{k}}+\mathcal{J}_0^2(2\lambda_0)\sin^2\theta_{\mathbf{k}}}\,,$$

where the anisotropy factor $f_0(\theta_{\mathbf{k}})$ for graphene is equivalent to our derived expression in Eq. (B22) with $\phi = 0$. This is an opposite limit for the angular dependence in Eq. (B22) compared to the dice lattice with $\phi = \pi/4$ and given by Eq. (B24). In addition, the two corresponding wave functions for graphene at $t = 0$ take the form

$$\Psi_d^{\gamma=\pm1}(\boldsymbol{k}) = \frac{1}{\sqrt{2}} \begin{bmatrix} 1 \\ \gamma\, \mathsf{e}^{i\Phi_0(\theta_{\mathbf{k}})} \end{bmatrix} , \tag{35}$$
$$\Phi_0(\theta_{\mathbf{k}}) = 2\arctan\left\{ \frac{\mathcal{J}_0(\lambda_0)\sin\theta_{\mathbf{k}}}{\cos\theta_{\mathbf{k}} + f_0(\theta_{\mathbf{k}})} \right\} \backsimeq \theta_{\mathbf{k}} - \frac{\lambda_0^2}{2}\,\sin(2\theta_{\mathbf{k}}) + \cdots .$$

As expected for a distorted anisotropic Dirac cone, its wave function in Eq. (35) possesses an equal amplitude for two components, while their renormalized phase factor $\Phi_0(\theta_{\mathbf{k}})$ depends on the interaction coefficient λ_0.

For the most general case of an α-T_3 lattice, its wave function is obtained as

$$\Psi_d^{\gamma=\pm1}(\boldsymbol{k}|\,\tau,\phi) = \frac{1}{\sqrt{\mathcal{N}_1(\boldsymbol{k}|\,\tau,\phi)}}\,\mathsf{e}^{\mp i v_F k f(\theta_{\mathbf{k}}|\,\phi)t} \tag{36}$$
$$\times \left\{ \frac{r_{11}(\boldsymbol{k}|\,\phi)}{\sqrt{2}} \begin{bmatrix} \tau\,\cos\phi \\ \pm 1 \\ \tau\,\sin\phi \end{bmatrix} \mathsf{e}^{\pm i z_\lambda(t)} + r_{12}(\boldsymbol{k}|\,\tau,\phi) \begin{bmatrix} \sin\phi \\ 0 \\ -\cos\phi \end{bmatrix} + \frac{r_{13}(\boldsymbol{k}|\,\tau,\phi)}{\sqrt{2}} \begin{bmatrix} \tau\cos\phi \\ \mp 1 \\ \tau\sin\phi \end{bmatrix} \mathsf{e}^{\mp i z_\lambda(t)} \right\} ,$$

where the coefficients $r_{11}(\boldsymbol{k}|\,\phi)$, $r_{12}(\boldsymbol{k}|\,\tau,\phi)$, $r_{13}(\boldsymbol{k}|\,\tau,\phi)$ and the normalization function $\mathcal{N}_1(\boldsymbol{k}|\,\tau,\phi)$ are defined in Appendix B.

For the flat band with $\gamma = 0$, the wave function takes the form

$$\Psi_d^{\gamma=0}(\boldsymbol{k}|\,\tau,\phi) = \frac{1}{\sqrt{2\mathcal{N}_0(\boldsymbol{k}|\,\phi)}} \left\{ \frac{r_{01}(\boldsymbol{k}|\,\phi)\,\tau}{\sqrt{2}} \sum_{\alpha=\pm1} \mathsf{e}^{i\alpha z_\lambda(t)} \begin{bmatrix} \cos\phi \\ \alpha\tau \\ \sin\phi \end{bmatrix} + r_{02}(\boldsymbol{k}|\,\phi) \begin{bmatrix} \sin\phi \\ 0 \\ -\cos\phi \end{bmatrix} \right\} , \tag{37}$$

where

$$r_{01}(\boldsymbol{k}|\,\phi) = -i\sin(2\phi)\sin\theta_{\mathbf{k}}\,\mathcal{J}_0(\lambda_0) , \tag{38}$$
$$r_{02}(\boldsymbol{k}|\,\phi) = \sqrt{2}\,[\cos\theta_{\mathbf{k}} + i\tau\cos(2\phi)\sin\theta_{\mathbf{k}}\,\mathcal{J}_0(2\lambda_0)] .$$

The components of the wave function in Eq. (37) are not equal to each other since this condition does not hold true even in the absence of irradiation, while all the previously obtained wave functions have components which differ only by a phase factor. This becomes explicit once the components of this wave function are reformulated as

$$\Psi_d^0(\lambda_0,\mathbf{k}) = \frac{1}{\sqrt{\mathcal{N}^0_{(\phi)}(\lambda_0,\theta_{\mathbf{k}})}} \begin{Bmatrix} \sin\phi\,\left[\cos\theta_{\mathbf{k}} - i\tau\,\sin\theta_{\mathbf{k}}\,\mathbb{X}_\theta^{(\phi)}(\lambda_0)\right] \\ 0 \\ -\cos\phi\,\left[\cos\theta_{\mathbf{k}} + i\tau\,\sin\theta_{\mathbf{k}}\,\left(2\,\mathcal{J}_0(\lambda_0) - \mathbb{X}_\theta^{(\phi)}(\lambda_0)\right)\right] \end{Bmatrix} , \tag{39}$$
$$\mathbb{X}_\theta^{(\phi)}(\lambda_0) = 2\cos^2\phi\,\mathcal{J}_0(\lambda_0) - \cos(2\phi)\,\mathcal{J}_0(2\lambda_0) \backsimeq 1 - \frac{\lambda_0^2}{4}\,[1 - 3\cos(2\phi)] ,$$
$$2\,\mathcal{J}_0(\lambda_0) - \mathbb{X}_\theta^{(\phi)}(\lambda_0) \backsimeq 1 - \frac{\lambda_0^2}{4}\,[1 + 3\cos(2\phi)] ,$$
$$\mathcal{N}^0_{(\phi)}(\lambda_0,\theta_{\mathbf{k}}) = \cos^2\theta_{\mathbf{k}} + \sin^2\theta_{\mathbf{k}} \left\{ \left[\sin\phi\;\mathbb{X}_\theta^{(\phi)}(\lambda_0)\right]^2 + \left[\cos\phi\,\left\{2\mathcal{J}_0(\lambda_0) - \mathbb{X}_\theta^{(\phi)}(\lambda_0)\right\}\right]^2 \right\} \backsimeq$$
$$\backsimeq 1 - \frac{\lambda_0^2}{4}\,\sin^2\theta_{\mathbf{k}}\,[5 + 3\cos(4\phi)] + ...$$

Here, for the most straightforward case of a flat band, we can explicitly demonstrate how the wave function is changed in the presence of linearly polarized irradiation, yielding

$$\Psi_d^{\gamma=0}(\lambda_0,\mathbf{k}) \backsimeq \frac{1}{\sqrt{\mathcal{N}^0_{(\phi)}(\lambda_0,\theta_{\mathbf{k}})}} \left\{ \begin{bmatrix} \sin\phi\, \mathsf{e}^{-i\tau\theta_{\mathbf{k}}} \\ 0 \\ -\cos\phi\ \mathsf{e}^{i\tau\theta_{\mathbf{k}}} \end{bmatrix} + i\tau\, \frac{\lambda_0^2}{4}\, \sin\theta_{\mathbf{k}} \begin{bmatrix} \sin\phi\,\{1-3\cos(2\phi)\} \\ 0 \\ \cos\phi\,\{1+3\cos(2\phi)\} \end{bmatrix} + ... \right\}, \tag{40}$$

$$\mathcal{N}^0_{(\phi)}(\lambda_0,\theta_{\mathbf{k}}) \backsimeq 1 - \frac{\lambda_0^2}{4}\, \sin^2\theta_{\mathbf{k}}\,\{5+3\cos(4\phi)\} + ... \ .$$

Obviously, the components of this wave function are not equal to each other, in contrast to all previously considered cases involving a linearly polarized field. The way they are modified in the presence of electron-photon interaction is not correlated with their initial values. The normalization factors for all obtained wave functions in both Eqs. (29), (32) and in Eqs. (36), (37) do not depend on time. It is quite simple to show that in the case of zero electron-light interaction $\lambda_0 \to 0$, the wave function in Eq. (36) is equivalent to that of non-irradiate α-T_3, given by Eq. (2). However, one should also keep in mind that the results for the wave function components are determined only to a finite complex phase factor.

III. FIELD-INDUCED MODIFICATION OF THE BERRY PHASES, CONNECTIONS AND CURVATURES

As an application of our derived photon-dressed electronic states in Sec. II, we explore how the Berry phase of an α-T_3 or a dice lattice is affected in the presence of an off-resonance dressing field with different polarizations. Specifically, we are interested in studying its dependence on geometry α and coupling λ_0 parameters.

We are also going to calculate the Berry connections and curvatures in vareious α-T_3 materials and demonstrate that for the case of linearly polarized field, the Chern number always remains zero, and a topological phase transition between a semimetal and Haldane insulator does not take place.

The Berry phase is defined as a geometrical phase difference, which a purely quantum system receives over a complete cycle of adiabatic, or isoenergetic evolution. [54–56] All physically meaningful parameters, except for a quantum phase, are expected to return to their initial values over such a loop-like transformation. The Berry phase is logically connected to a jump of the *Aharonov and Bohm* phase for a charged particle moving along an arbitrary closed path, which partially includes either electrostatic or magnetic field. Such a topological phase can strongly affect transport properties and lead to a finite conductivity at the band crossing even if the density of propagating waves at this point vanishes. [57]

As a first step to this study, we are going to carry out a detailed investigation of the time-independent eigenstates, corresponding to the distorted Dirac cone due to strong interaction of electrons with an optical field. This could lead to either opening a band gap under an elliptically or circularly polarized field or creating an anisotropy in the dispersion relations due to the presence of linearly polarized light. While in the former case the energy dispersion in Eq. (18) are obtained by using a time-independent effective perturbation Hamiltonian in Eq. (10), the wave functions for the latter case involving linearly polarized light acquire a complete time dependence, and therefore need to be clarified further. Such a picture could be regarded as a simplified model with an additional $\hat{\Sigma}_z$ Hamiltonian term for graphene under circularly polarized light [17], which provides some insights to our considered phenomena including irradiated graphene. [34] We will suppress the time dependence in Eqs. (36) and (37) by using their expressions at $t = 0$ for all further computations. This allows us to address a wider class of field-induced electronic states, not necessarily equivalent to dressed states under conditions discussed above.

In most cases, the time dependence in the obtained eigenstates, such as Eqs. (36) and (37), takes an exponential form $\mathtt{exp}[\pm i\lambda_0 \sin(\omega t)]$ in some of their components. For our case with an off-resonant field $\lambda_0 \ll 1$, this dependence would produce noticeable modification to these wave function components. Surprisingly, the normalization factors $\mathcal{N}_{0,1}(\boldsymbol{k})$ for all types of α-T_3 materials under linearly polarized irradiation, including the dice lattice limit, do not depend on time. Another direct time dependence is in the initial phase factor $\mathtt{exp}\,[\mp i v_F k t f(\theta_{\mathbf{k}})]$ of Eqs. (36) and (29), which does not affect most of its physical properties but leads to a linear increase of its Berry phase $\propto v_F k t f(\theta_{\mathbf{k}})$.

The described situation of the time dependence above is strikingly similar to the *electrostatic Aharonov-Bohm interference* effect. [58] The wave function of a conventional Schrődinger particle of energy $\mathbb{E}$ has a phase factor $\mathtt{exp}[i\phi]$ with $\phi = -\mathbb{E}t/\hbar$. If such a particle is confined in the region with a constant electrostatic potential V_0, and then a zero electrostatic field, this potential produces an additional phase $\phi(t) - \phi(t=0) = -eV_0 t/\hbar$ to its eigenstate, which can influence actual properties of the particle and the outcome of a double-slit interference experiment.

As is well known, we can write down a general expression for Berry phase $\Phi_B(\gamma, \boldsymbol{k}|\,\tau,\phi)$ as [55,56]

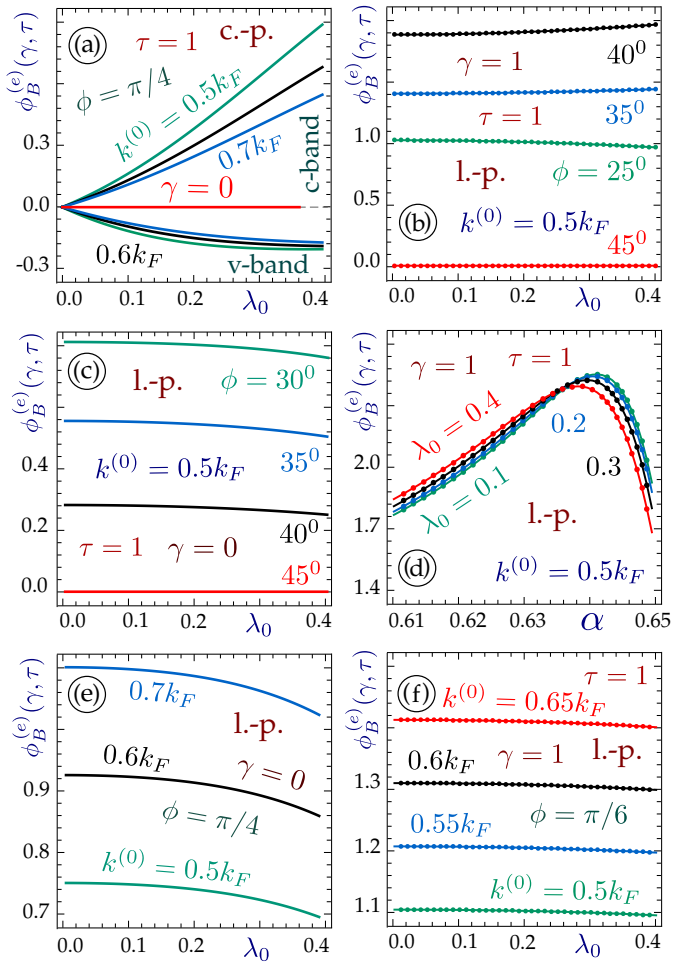

FIG. 6: (Color online) Numerically calculated Berry phase $\Phi_B^{(e)}(\gamma, \boldsymbol{k}|\,\tau, \phi)$ from Eq. (41) for irradiated α-T_3 lattices at $\tau = 1$ valley. Panel (a) corresponds to circularly polarized light (labeled by c), while panels (b)-(f) correspond to linearly polarized light (labeled by L). Panel (a) presents $\phi_B^{(c)}(\gamma, |\boldsymbol{k}| = k_0|\,\phi)$ having $\beta = 1$ with $\phi = \pi/4$ for $\gamma = 1$ (three positive curves), $\gamma = 0$ (middle red curve), $\gamma = -1$ (three negative curves), where $k_0/k_F = 0.5$, 0.6, 0.7 are selected for green, black, blue curves. Berry phases $\Phi_B^{(L)}(\gamma, \boldsymbol{k}|\,\phi)$ having $\beta = \gamma = 0$ in plot (c) with $k_0/k_F \equiv 0.5$ and plot (e) with $\phi \equiv \pi/4$ on the left display λ_0 dependence for $\phi = 30^o$ (green), 35^o (blue), 40^o (black), 45^o (red) in panel (c) and for $k_0/k_F = 0.5$ (green), $k_0/k_F = 0.6$ (black), $k_0/k_F = 0.7$ (blue) in panel (e). All the right panels (b), (d), (f) are for $\beta = 0$ and $\gamma = 1$, where $k_0/k_F = 0.5$ is chosen in (b) to show λ_0 dependence for $\phi = 25^o$ (green), 35^o (blue), 40^o (black), 45^o (red); $k_0/k_F = 0.5$ is chosen in (d) to show α dependence for $\lambda_0 = 0.1$ (green), 0.2 (blue), 0.3 (black), 0.4 (red); and $\phi = \pi/4$ is chosen in (f) to show λ_0 dependence for $k_0/k_F = 0.5$ (green), 0.55 (blue), 0.6 (black), 0.65 (red).

$$\Phi_B(\gamma, \boldsymbol{k}|\,\tau, \phi) = -i \oint_{\mathbb{C}} d\boldsymbol{k} \cdot [\Psi_d^{\gamma}(\boldsymbol{k}|\,\tau, \phi)]^{\dagger}\, \boldsymbol{\nabla}_{\mathbf{k}} \Psi_d^{\gamma}(\boldsymbol{k}|\,\tau, \phi)\ , \tag{41}$$

where $\mathbb{C}$ represents an arbitrary closed path within a lattice plane. For the case of non-irradiated wave functions of an α-T_3 lattice presented in Eqs. (2) and (3), we immediately find the results as $\Phi_B(\gamma = \pm 1, \boldsymbol{k}|\,\tau, \phi) = \tau\pi\cos(2\phi)$ for the conduction and valence bands, and $\Phi_B(\gamma = 0, \boldsymbol{k}|\,\tau, \phi) = 2\pi\tau\cos(2\phi)$ for the flat band at two valleys. These conclusions *do not depend* on the choice of a closed curve $\mathbb{C}$, which in general cannot be true since the wave function components are $\boldsymbol{k}$ dependent. We also remark that the Berry phase is gauge invariant and its value is unique up to multiples of $\pm 2\pi$.

The details on how to evaluate the integral with respect to $\boldsymbol{k}$ in Eq. (41) using polar coordinates are provided in Appendix C for various types of incoming light polarization. In the case of circularly polarized light, components of the wave function are only k-dependent except for $\mathsf{e}^{\pm i\theta_{\mathbf{k}}}$ factors, which are similar to those for the non-irradiated eigenstates in Eqs. (2) and (3). Therefore, the path of such isoenergetic linear integration is a circle of radius k_0. As

a result, the Berry phase for a dice lattice irradiated by circularly polarized light takes the analytical expression as

$$\Phi_B^{(c)}(\gamma,k_0|\,\tau=1)=\frac{\mathcal{C}_1^2(\gamma,k_0)-1}{\mathcal{N}(\gamma,k_0)}\int_0^{2\pi}d\theta_{\mathbf{k}}\backsimeq\pi\,\frac{c_0}{\hbar v_F k^{(0)}}\,\lambda_0\left(\gamma+\frac{c_0}{\hbar v_F k_0}\,\lambda_0\right)\,. \tag{42}$$

These Berry phases are not symmetric, but opposite for electron and hole states except for the first-order term in the λ_0 expansion. However, this expression is symmetric for valleys, i.e., $\Phi_B^{(c)}(\gamma,k_0|\,\tau=-1)=-\Phi_B^{(c)}(\gamma,k_0|\,\tau=1)$, as seen in Fig. 6($a$), which is in analogy with the dice lattice in the absence of irradiation. [56] Even for a dice lattice which has a zero Berry phase, a finite Berry phase can still be established by an elliptically or a circularly polarized dressing field which opens an energy gap for the dice lattice. Although the dispersions in a dice lattice are symmetric, the wave function components, and therefore the Berry phases do not share this property. The corresponding phase for the flat band remains zero with respect to valley index and intensity of incoming radiation.

Finally, we have numerically calculated the Berry phase for the α-T_3 lattice with an arbitrary ϕ in the presence of linearly polarized radiation. Our numerical results are presented in Fig. 6. Panels (c) and (e) represent the results for the flat band, while the three right plots (b), (d) and (f) are for the conduction band. In both cases, the phase is zero for a dice lattice, disregarding the light intensity or the parameters k_0 of isoenergetic elliptic integral path so that all the curves in panel (d) approach zero in the limit of $\alpha\to 1$, which confirms our analytical result in Appendix C for a dice lattice under a linearly polarized dressing field. The results for the flat band demonstrate a stronger dependence on the coupling constant, as well as on the parameters k_0. As we see from Fig. 6(d), the λ_0 dependence of the Berry phase becomes non-monotonic for various α values. Such unique dependence has not been reported for the case of circularly polarized irradiation.

Recently, topological effects in connection with various optical phenomena have become a crucial research subject for photonic crystals, quasicrystals and metamaterials. In Ref. [59], the authors discussed creating interface supported new states of light based on topologies in wave-vector space and unidirectional waveguides that allow unimpeded propagation of light around large imperfections in a photonic crystal. An investigation on longitudinally-driven photonic lattices in connection with Lieb and kagome lattices, based on a tight-binding model, has been reported in Ref. [60]. A topological phase transition in α-T_3 materials under a circularly polarized irradiation was also addressed in a recent paper. [61] Consequently, in the present calculation, we will *focus solely on a linear polarization* for incoming light.

The Berry connection vector field $\mathbf{A}^{\gamma}_{\tau,\phi}(\mathbf{k},\lambda_0)$ and the Berry curvature $\mathbf{\Omega}^{\gamma}_{\tau,\phi}(\mathbf{k},\lambda_0)$ are defined as

$$\begin{aligned}&\mathbf{A}^{\gamma}_{\tau,\phi}(\mathbf{k},\lambda_0)\equiv\langle\Psi^{\gamma}_d(\mathbf{k},\lambda_0|\,\tau,\phi)|\,i\boldsymbol{\nabla}_{\mathbf{k}}\,|\Psi^{\gamma}_d(\mathbf{k},\lambda_0|\,\tau,\phi)\rangle\ ,\\&\mathbf{\Omega}^{\gamma}_{\tau,\phi}(\mathbf{k},\lambda_0)\equiv\boldsymbol{\nabla}_{\mathbf{k}}\times\mathbf{A}^{\gamma}_{\tau,\phi}(\mathbf{k},\lambda_0)\ .\end{aligned} \tag{43}$$

In the absence of incident light, the Berry connections for the cone bands with $\gamma=\pm1$ are $\mathbf{A}^{\gamma=\pm1}_{\tau,\phi}(\mathbf{k},\lambda_0)=+(\tau/2)\cos(2\phi)\,\boldsymbol{\nabla}_{\mathbf{k}}\theta_{\mathbf{k}}$ and $\mathbf{A}^{\gamma=0}_{\tau,\phi}(\mathbf{k},\lambda_0)=-2\mathbf{A}^{\gamma=\pm1}_{\tau,\phi}(\mathbf{k},\lambda_0)$ for the flat band. Here, the $\times2$ difference comes from the normalization of different wave functions.

In Appendix C, we show that without external irradiation [52]

$$\begin{aligned}&\mathbf{\Omega}^{\gamma=\pm1}_{\tau,\phi}(\mathbf{k},\lambda_0=0)=\tau\pi\,\cos(2\phi)\,\delta(\mathbf{k})\ ,\\&\mathbf{\Omega}^{\gamma=0}_{\tau,\phi}(\mathbf{k},\lambda_0=0)=-2\tau\pi\,\cos(2\phi)\,\delta(\mathbf{k})\ .\end{aligned} \tag{44}$$

The two-dimensional delta function $\delta(\mathbf{k})$ of a vector $\mathbf{k}$ has a dimension of $1/k^2$ and is expressed as $\delta(\mathbf{k})=\delta(k_x)\,\delta(k_y)=1/(2\pi k)\,\delta(k)$ if there is no angular dependence. Therefore, the Berry connection for a dice lattice *will always remain zero even in the presence of a linearly polarized dressing field.*

Now let us address a general case for α-T_3 lattices with an arbitrary α value within the range of $0<\alpha<1$. Here, however, the absolute values of non-zero components of a wave function are no longer equal to each other, not just different phase factors. In this general case, the wave function acquires a form $\Psi^{\gamma}_d(\lambda_0,\mathbf{k})=\{c_1^{\gamma},c_2^{\gamma},c_3^{\gamma}\}^{\mathbb{T}}$ with its three components $c_i^{\gamma}\equiv c_i^{\gamma}(\tau,\phi\,|\,\theta_{\mathbf{k}},\lambda_0)$ for $i=1,\,2,\,3$.

Therefore, the Berry field for $\gamma=0$ is calculated as

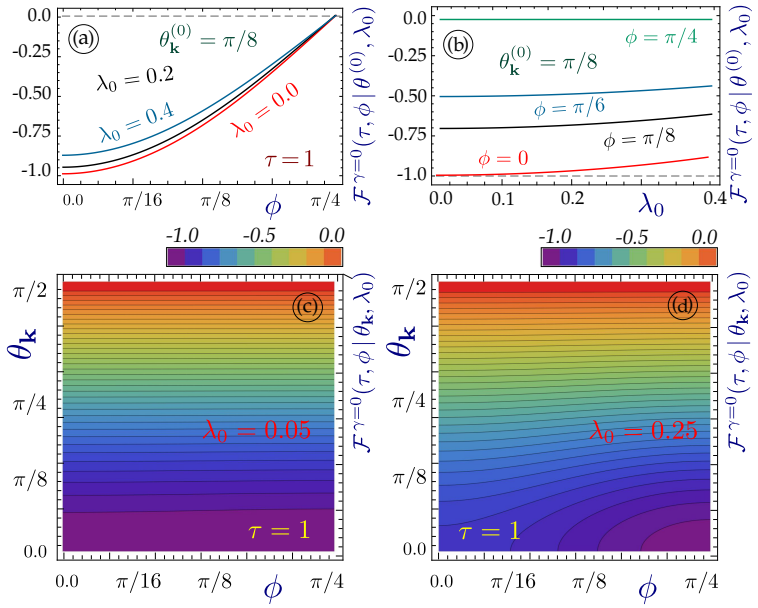

FIG. 7: (Color online) Angular factor $\mathcal{F}^{\gamma=0}(\tau,\phi\,|\,\theta_{\mathbf{k}},\lambda_0)$ from Eq. (45) for the flat band with $\gamma = 0$ at the $\tau = 1$ valley under a finite electron-light interaction $0 < \lambda_0 \ll 1$. Panel (a) shows the dependence of $\mathcal{F}^{\gamma=0}$ on the geometry phase ϕ at $\theta_{\mathbf{k}} = \pi/8$, where each curve represents different λ_0 values. Panel (b) demonstrates its dependence on λ_0 at $\theta_{\mathbf{k}} = \pi/8$ for various phases ϕ. Contour plots (c) and (d) display $\mathcal{F}^{\gamma=0}$ as a function of both angle $\theta_{\mathbf{k}}$ and phase ϕ, where $\lambda_0 = 0.05$ and $\lambda_0 = 0.25$ are assumed, respectively, in (c) and (d).

$$\mathbf{A}^{\gamma=0}_{\tau,\phi}(\mathbf{k},\lambda_0) = \frac{1}{k}\,\mathcal{F}^{\gamma=0}(\tau,\phi\,|\,\theta_{\mathbf{k}},\lambda_0)\,\hat{e}_\theta\ ,$$
$$\mathcal{F}^{\gamma=0}(\tau,\phi\,|\,\theta_{\mathbf{k}},\lambda_0) = \sum_{i=1}^{3}\left(c_i^{\gamma=0}\right)^*\,\frac{\partial c_i^{\gamma=0}}{d\theta_{\mathbf{k}}}\ . \tag{45}$$

For this case, the derivation is greatly simplified due to the fact that each component and the normalization factor of the states (including those for $\gamma = \pm 1$) only depend on the angle $\theta_{\mathbf{k}}$. The next step is the derivative of $\mathbf{A}^{\gamma=0}_{\tau,\phi}(\mathbf{k},\lambda_0)$ with respect to k, which leads to an additional delta function, while the k-dependent term is kept unchanged.

Finally, the Berry curvature is found to be

$$\mathbf{\Omega}^{\gamma=0}_{\tau,\phi}(\mathbf{k},\lambda_0) = \frac{1}{k}\,\frac{\partial}{\partial k}\left[k(A^{\gamma=0}_{-,\phi})_\theta\right]\hat{e}_z = \frac{\delta(k)}{k}\,\mathcal{F}^{\gamma=0}(\tau,\phi\,|\,\theta_{\mathbf{k}},\lambda_0)\,\hat{e}_z\ . \tag{46}$$

Similar results can be obtained for $\gamma = \pm 1$ wave functions. Since there is an angular dependence and $\mathcal{F}^{\gamma}(\tau,\phi\,|\,\theta_{\mathbf{k}},\lambda_0)$ becomes anisotropic in Eq. (45), the identity $\delta(k)/k = 2\pi\delta(\mathbf{k})$ can not be applied to $\mathcal{F}^{\gamma}(\tau,\phi\,|\,\theta_{\mathbf{k}},\lambda_0)$ anymore.

We see from Figs. 7 and 8 that the obtained angular factor is only slightly modified by the presence of a dressing field because we only consider the weak-coupling case with $\lambda_0 \ll 1$. This agrees with the assumption that the field frequency lies within the off-resonance region. In addition, the anisotropic dependence of $\mathcal{F}$ on $\theta_{\mathbf{k}}$, as well as in other observable quantities, appears only under an irradiation since its isotropic dependence in the $\lambda_0 \to 0$ limit can be verified directly from Eq. (44). From panels (a) and (b) of both figures, we can further verify $\mathcal{F}^{\gamma} = 0$ for dice lattice ($\phi = \pi/4$) even with an electron-light interaction. The results for $\gamma = -1$ are not shown here since they are nearly the same as those for $\gamma = 1$ in Fig. 8. The ϕ dependence becomes visible only for ϕ close to 0 or $\pi/4$ and small $\theta_{\mathbf{k}}$ with an enhanced electron-light coupling in Figs. 7(d) and 8(d). For $\lambda_0 \to 0$, on the other hand, the results for $\gamma = \pm 1$ become half of that for $\gamma = 0$ with an opposite sign, as predicted by Eq. (44).

For all three bands and allowable intensities of an imposed irradiation, the most important observed feature is that the Berry curvature always retains the valley symmetry, i.e., $\mathbf{\Omega}^{\gamma}_{\tau,\phi}(\mathbf{k},\lambda_0)$ is proportional to τ, just as we have found in Eq. (44) for a non-irradiated α-T_3. In contrast to the previously studied case, the current work clearly indicates

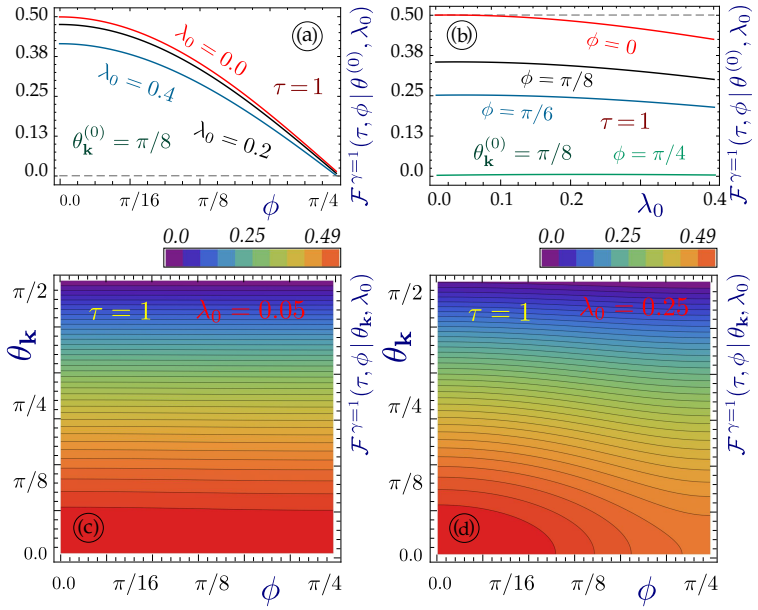

FIG. 8: (Color online) Calculated $\mathcal{F}^{\gamma=1}(\tau, \phi \,|\, \theta_{\mathbf{k}}, \lambda_0)$ for $\tau = 1$ under a finite electron-light interaction, where all the parameters, panels and curves are presented in the same way as in Fig. 7.

that a linearly polarized dressing field *can not change the Chern number* of α-T_3 materials due to its conserved valley symmetry. This conclusion can be compared with bilayer graphene as discussed in Ref. [62]. However, our results for both Berry connection and curvature are very useful for exploring the electronic properties of crystalline solids. [55] We also need to point out that in the case of linearly polarized irradiation there is no breaking of time reversal symmetry.

Now we are ready to analyze the way in which the topological properties of α-T_3 materials are modified by a dressing field. For all types of irradiation which open a finite bandgap, a semimetal is transformed into a Chern insulator, accompanied by a phase transition. This includes the case for a circularly polarized irradiation with $\beta = 1$, as described in the above mentioned Arxiv preprint by B. Dey and K. Ghosh, and the case for a general elliptic polarization with $0 < \beta < 1$, where $0 < \beta < 1$ is the ratio of field strengths along the two axes of a polarization ellipse, introduced in Eq. (4) and discussed below. Since two obtained bandgaps, given by Eqs. (11) and (12), are proportional to βc_0, the Chern number would always be varied, as long as at least one or two gaps occur in the energy dispersions of a material considered.

On the contrary, in the opposite limit of $\beta \to 0$ for a linearly polarized dressing field, the Chern number can not be changed and remains to be zero due to the valley symmetry remained in the calculated Berry curvature. Using this unique feature, one is able to manage a tunable topological phase transition in an actual optoelectronic device.

IV. CONCLUDING REMARKS

In this paper, we have executed a thorough investigation into electron-photon dressed states in α-T_3 lattices for all possible polarizations (elliptical, circular and linear) of the impinging radiation. We have derived closed-form expressions and analytic approximations of the quasiparticle energy dispersions for all types of such optical states.

We have demonstrated that the geometry phase ϕ or the hopping-scale parameter α plays a crucial role and affects the low-energy band structure for various types of polarizations of incident light. The obtained dressed states demonstrate both similarity and strong distinction compared to those earlier results obtained for graphene or buckled honeycomb lattices. As an example, elliptically polarized irradiation is connected to opening a bandgap in the energy dispersions of α-T_3 lattices, as well as symmetry breaking between the valence and conduction bands. For the case with a linearly polarized light field, the parameter α has also been shown to modify significantly the radiation-induced anisotropy and the angular dependence of the dressed quasiparticle dispersions in $\boldsymbol{k}$ space. Generally speaking, we find that the band-structure anisotropy due to electron-light coupling becomes the strongest for graphene with $\alpha \to 0$ and the weakest for a dice lattice with $\alpha = 1$ for both circular and linear polarizations of incoming light.

We have also found that for an elliptically polarized field applied to α-T_3 lattices with $\alpha \neq 1$, its low-energy band structure, including opened bandgaps, explicitly depends on the valley indexes $\tau = \pm 1$. This gives rise to valleytronics applications, which now could be developed based on irradiated α-T_3 lattices and enables electrically-controlled valley filtering as a milestone for such technologies and applications.

In addition to calculated energy dispersion relations, we have analytically obtained the corresponding wave function for electrons dressed by an optical field with different polarizations. For elliptically polarized light, the components of eigenstates obtained are shown to be inequivalent beyond a simple phase factor as seen from Eqs. (2) and (3) in the absence of irradiation. Instead, these components depend on both the wave-vector $\boldsymbol{k}$ and the band index γ. As a result, the modifications to the eigenstates of the valence, conduction and flat bands are completely different. Our current study presents the first explicit expression for the dressed-state wave function of a dice lattice with an opened energy gap under external irradiation.

Unlike the previous discussion for circularly polarized irradiation, our obtained eigenvalue equation, including a linearly polarized dressing field, permits an exact solution for energy dispersions with respect to $\boldsymbol{k}$. This leads us to the following conclusions: (i) there is no energy gap between the conduction and valence bands; (ii) the flat band stays forever at zero energy; (iii) a complete symmetry between conduction and valence bands is retained. However, the presence of linearly polarized dressing induces an α-dependent anisotropy of the Dirac cone in $\boldsymbol{k}$ space, similar to graphene. Therefore, we are able to tune the anisotropy and angular dependence of the energy band structure by adjusting the hopping-scale parameter α. Although some discussions on the breaking of band symmetry in the irradiated α-T_3 model were reported earlier in Ref. [2], we reveal a number of other crucial symmetries in the dressed states, and more importantly, these symmetries could be either broken or retained depending on the type and intensity of the selected dressing field and on the value of hopping-scale parameter α.

Throughout the paper, we have continually compared our results with the limiting case of a dice lattice for which $\alpha = 1$ or $\phi = \pi/4$. Due to the fact that dice lattices were discovered much earlier than α-T_3 and could be synthesized in a relative easy way, there has already been a substantial amount of research effort devoted specifically to the dice, such as Ref. [1]. In contrast with general α-T_3 materials, the dice lattice preserves the valence/conduction band symmetry under irradiation of any polarization. Only because of this unusual property, the electronic states could be presented in such a concise way. Our results suggest that in the presence of a linearly polarized irradiation, each component of the wave function only receives an additional phase depending on the electron-light coupling. Therefore, the actual complex phase is no longer equivalent to the wave vector angle $\theta_{\mathbf{k}}$, as shown in Eq. (33). Consequently, all observables, such as, electron momentum, current, etc., will be modified in a specific and predictable way.

The wave functions are shown to be drastically different for the dice lattice ($\alpha = 1$) and all other possible α-T_3 lattices ($\alpha \neq 1$). In the former case, the wave function components of such a dressed state are equivalent and differ only by a phase factor, which are similar to anisotropic Dirac fermions in few-layer black phosphorus [35] and expected to reveal non-head-on asymmetric Klein paradox. In contrast, the wave function components for arbitrary $0 < \alpha < 1$ differ from each other beyond a simple phase factor, which will bring in considerable modifications to tunneling and transport properties in general α-T_3 lattices. Particularly, to highlight such imbalance in components, we also present explicit initial wave functions at $t = 0$ to elucidate a wider class of phenomena pertaining to light-induced distortions in Dirac cone dispersions for general α-T_3 lattices.

We investigates the Berry phases of dressed electron eigenstates in connection with their unusual composition and symmetric properties. The Berry phase is shown to be a specific quantum characteristic of an electronic state, which is greatly sensitive to a particle's environment and adiabatic change of external fields or their potentials.

Berry phases are directly related to the wave function $\boldsymbol{k}$ dependence, its components and the phase difference between them. For instance, the phases corresponding to the valence and conduction bands for a gap-opening elliptically- or circularly polarized irradiation for the simplest dice lattice are not just different by an opposite, quite different from their energy dispersions. We have uncovered the complex connection between dressed states of conduction and valence bands and demonstrated a zero phase for the flat-band electronic state. For a dice lattice with $\phi = \pi/4$, the Berry phases are all zero for three bands even in the presence of linearly polarized light. For all other values of $\phi \neq \pi/4$, on the other hand, we have found moderate dependence of Berry phase on electron-light coupling λ_0, hopping-scale parameter α and the selection of closed integration path as expected from the Aharonov-Bohm effect. We have noted that modified Berry phases by specific electron-light coupled states can affect some important physical properties of a system, e.g., results of a double-slit interference experiment.

We have also calculated the Berry connections and curvatures for the case of linearly polarized irradiation and demonstrated that for linear polarization, which does not lead to the creation of a finite bandgap, the Chern numbers remain to be zero and topological phase transition will not occur.

In closing, by studying the band structure of such dressed electron states, we have developed a useful methodology for laser-induced engineering of energy bands and dressed electronic states, as well as tuning most significant characteristics of α-T_3 innovative materials. Our results in this paper are expected to have a profound influence on the fabrication of modern optoelectronic and photonic devices.

Acknowledgments

D.H. would like to acknowledge the support from the Air Force Office of Scientific Research (AFOSR). D.H is also supported by the DoD Lab-University Collaborative Initiative (LUCI) program. G.G. would like to acknowledge the support from the Air Force Research Laboratory (AFRL) through Grant #12530960.

Appendix A: Electron-field dressed states for elliptically- and circularly-polarizations applied to a dice lattice ($\phi = \pi/4$)

For a dice lattice, the time-independent perturbation operator introduced in Eq. (9) is

$$\hat{\mathbb{P}}_{\tau} = -\frac{\tau c_0}{2\sqrt{2}} \sum_{\alpha=\pm} (1 - \alpha\tau\beta)\, \hat{\Sigma}_{\alpha}^{(1)} \ , \tag{A1}$$

where we have defined

$$\hat{\Sigma}_{+}^{(1)} = \begin{bmatrix} 0 & \hat{\mathbb{I}}_{2\times 2} \\ 0 & 0\ 0 \end{bmatrix} = \begin{bmatrix} 0 & 1 & 0 \\ 0 & 0 & 1 \\ 0 & 0 & 0 \end{bmatrix} \qquad \text{and} \qquad \hat{\Sigma}_{-}^{(1)} = \begin{bmatrix} 0\ 0 & 0 \\ \hat{\mathbb{I}}_{2\times 2} & 0 \end{bmatrix} = \begin{bmatrix} 0 & 0 & 0 \\ 1 & 0 & 0 \\ 0 & 1 & 0 \end{bmatrix} \ . \tag{A2}$$

The operators $\hat{\Sigma}_{\pm}^{(1)}$ can be built from the spin-1 matrices

$$\hat{\Sigma}_{x}^{(1)} = \frac{1}{\sqrt{2}} \begin{bmatrix} 0 & 1 & 0 \\ 1 & 0 & 1 \\ 0 & 1 & 0 \end{bmatrix} \qquad \text{and} \qquad \hat{\Sigma}_{y}^{(1)} = \frac{1}{\sqrt{2}} \begin{bmatrix} 0 & -i & 0 \\ i & 0 & -i \\ 0 & i & 0 \end{bmatrix} \ , \tag{A3}$$

and $\hat{\Sigma}_{\pm}^{(1)} = \hat{\Sigma}_{x}^{(1)} \pm i\hat{\Sigma}_{y}^{(1)}$, similarly to the case of 2×2 Pauli matrices for spin-1/2 used for graphene. Moreover, the energy gap exists if a $\hat{\Sigma}_{z}^{(1)}$ matrix is present in the Hamiltonian. For our case, this matrix is in the form

$$\hat{\Sigma}_{z}^{(1)} = \frac{1}{\sqrt{2}} \begin{bmatrix} 1 & 0 & 0 \\ 0 & 0 & 0 \\ 0 & 0 & -1 \end{bmatrix} \ . \tag{A4}$$

Using the above results in Eqs. (A1)-(A4), from Eq. (8) we get the effective pertubation Hamiltonian presented in Eq. (10)

$$\hat{\mathcal{H}}_{\text{eff}}^{(e)}(\boldsymbol{k}|\,\tau) = \frac{\hbar v_F}{\sqrt{2}} \sum_{\alpha=\pm} (\tau k_x - i\alpha k_y)\, \Sigma_{\alpha}^{(1)} - \frac{\tau\beta}{2}\, \lambda_0\, \hat{\Sigma}_{z}^{(1)} + \frac{\tau\hbar v_F}{4\sqrt{2}\lambda_0^2} \sum_{\alpha=\pm} \left(\beta^2\tau k_x - i\alpha k_y\right)\, \Sigma_{\alpha}^{(1)} \ . \tag{A5}$$

Furthermore, for the Hamiltonian in Eq. (A5), we arrive at the following eigenvalue equation for energy-band dispersions $\varepsilon_{d}^{(e)}(\boldsymbol{k}|\,\tau)$

$$\left[\varepsilon_{d}^{(e)}(\boldsymbol{k}|\,\tau)\right]^3 - \left(\frac{\beta c_0 \lambda_0}{2}\right)^2 \varepsilon_{d}^{(e)}(\boldsymbol{k}|\,\tau) - (\hbar v_F)^2 \left\{ \left[1 + \left(\frac{\beta\lambda_0}{2}\right)^2\right]^2 k_x^2 + \left[1 + \left(\frac{\lambda_0}{2}\right)^2\right]^2 k_y^2 \right\} \varepsilon_{d}^{(e)}(\boldsymbol{k}|\,\tau) = 0 \ . \tag{A6}$$

Here, we see the dispersions $\varepsilon_d^{(e)}(\boldsymbol{k}|\,\tau)$ acquire a complete e-h symmetry and a *renormalized isotropic* Fermi velocity $\bar{v}_F$ given by

$$\bar{v}_F = v_F\left[1+\frac{\lambda_0^2}{2}\left(1+\frac{\lambda_0^2}{8}\right)\right] = v_f\left[1+\left(\frac{\lambda_0}{2}\right)^2\right]^2 , \tag{A7}$$

and we will omit the λ_0 dependence hereafter in other expressions for simplicity.

Appendix B: Linearly polarized irradiation on a α-T_3 lattice

First, the total Hamiltonian of a quasiparticle interacting with linearly polarized field is

$$\hat{\mathcal{H}}(\boldsymbol{k},t|\,\tau,\phi) = \hat{\mathbb{H}}_\tau^\phi(\boldsymbol{k}) + \hat{\mathbb{H}}_A^{(L)}(t|\,\tau,\phi) , \tag{B1}$$

which contains an additional time-dependent interaction term

$$\hat{\mathbb{H}}_A^{(L)}(t|\,\tau,\phi) = -\tau c_0\cos(\omega t)\begin{bmatrix} 0 & \cos\phi & 0 \\ \cos\phi & 0 & \sin\phi \\ 0 & \sin\phi & 0 \end{bmatrix} , \tag{B2}$$

where the coupling amplitude $c_0 = eE_0v_F/\omega$ is identical to that in the case of elliptically- or circularly polarized light. Therefore, for $\boldsymbol{k}=0$, and then $\hat{\mathbb{H}}_\tau^\phi(\boldsymbol{k})=0$, the Schrődinger equation becomes

$$i\hbar\frac{d\psi_0(t|\,\tau,\phi)}{dt} = \hat{\mathbb{H}}_A^{(L)}(t|\,\tau,\phi)\,\psi_0(t|\,\tau,\phi) . \tag{B3}$$

The solutions of Eq. (B3) for the valence and conduction bandedges with $\gamma=\pm1$ at $\boldsymbol{k}=0$ are

$$\psi_0^{\gamma=\pm1}(t|\,\tau,\phi) = \frac{1}{\sqrt{2}}\begin{bmatrix} \tau\cos\phi \\ \pm1 \\ \tau\sin\phi \end{bmatrix} \mathsf{e}^{\pm i\lambda_0\sin(\omega t)} , \tag{B4}$$

and for the flat band with $\gamma=0$ is

$$\psi_0^{\gamma=0}(t|\,\tau,\phi) = \begin{bmatrix} \sin\phi \\ 0 \\ -\cos\phi \end{bmatrix} . \tag{B5}$$

The wave functions in Eqs. (B4) and (B5) are obviously orthonormal to each other and these expressions respectively resemble the $\boldsymbol{k}$-dependent results in Eqs. (2) and (3) in the absence of light interaction.

The next step is to extend our solution for $\boldsymbol{k}=0$ to a finite wave-vector $\boldsymbol{k}$. For this purpose, we would solve the following time-dependent Schrődinger equation

$$i\hbar\,\frac{\partial}{\partial t}\Psi(\boldsymbol{k},t|\,\tau,\phi) = \hat{\mathcal{H}}(\mathbf{k},t|\,\tau,\phi)\,\Psi(\boldsymbol{k},t|\,\tau,\phi) \tag{B6}$$

for the full Hamiltonian in Eq. (B1). We look for its solution in the following expansion form

$$\Psi(\boldsymbol{k},t|\,\tau,\phi) = \sum_\gamma \mathcal{F}^{(\gamma)}(\boldsymbol{k},t|\,\tau,\phi)\,\psi_0^\gamma(t|\,\tau,\phi) , \tag{B7}$$

in which $\gamma=0,\,\pm1$ and the unknown time- and $\boldsymbol{k}$-dependent expansion coefficients $\mathcal{F}^{(\gamma)}(\boldsymbol{k},t)$ need to be determined. By using Eq. (B3) for $\boldsymbol{k}=0$ and the orthogonality of $\psi_0^\gamma(t|\,\tau,\phi)$, Eq. (B6) can be rewritten perturbatively as

$$i\hbar\,\frac{\partial}{\partial t}\mathcal{F}^{(\gamma)}(\boldsymbol{k},t|\,\tau,\phi)=\sum_{\rho}\mathcal{F}^{(\rho)}(\boldsymbol{k},t|\,\tau,\phi)\,\langle\psi_0^{\gamma}(t|\,\tau,\phi)\,|\,\hat{\mathbb{H}}_{\tau}^{\phi}(\boldsymbol{k})\,|\,\psi_0^{\rho}(t|\,\tau,\phi)\rangle\ . \tag{B8}$$

This leads to three coupled linear partial-differential equations

$$\begin{aligned}
&\frac{i}{v_F}\,\frac{\partial}{\partial t}\mathcal{F}^{(\mp1)}=\mp k_x\,\mathcal{F}^{(\mp1)}\mp\frac{i}{\sqrt{2}}\,\mathsf{e}^{\pm iz_\lambda(t)}\sin(2\phi)\,k_y\,\mathcal{F}^{(0)}\mp i\mathsf{e}^{\pm2iz_\lambda(t)}\,\tau\cos(2\phi)\,k_y\,\mathcal{F}^{(\pm1)}\,,\\
&\frac{\partial}{\partial t}\mathcal{F}^{(0)}=\frac{v_F}{\sqrt{2}}\,\sin(2\phi)\,k_y\sum_{\alpha=\pm1}\alpha\,\mathsf{e}^{-i\alpha z_\lambda(t)}\,\mathcal{F}^{(-\alpha)}\ ,
\end{aligned} \tag{B9}$$

where $z_\lambda(t)=\lambda_0\sin(\omega t)$ and we omit the $\boldsymbol{k}$ and t dependence in $\mathcal{F}^{(\gamma)}$ for simplicity. Using Floquet theorem, we look for the dressed state in the form of [2,17,34]

$$\mathcal{F}^{(\gamma)}(\boldsymbol{k},t|\,\tau,\phi)=\mathsf{exp}\left\{-\frac{i}{\hbar}\,\varepsilon_d(\boldsymbol{k}|\,\tau,\phi)\,t\right\}\sum_{n=-\infty}^{\infty}f_n^{(\gamma)}\mathsf{e}^{in\omega t}\ , \tag{B10}$$

where $\varepsilon_d(\boldsymbol{k}|\,\tau,\phi)$ represents the dressed-state energy dispersion to be decided. The second factor in Eq. (B10) is a periodic function of time (with the period $T_0=2\pi/\omega$), which can be expanded in a Fourier series. A nested exponential function is traditionally reduced by the Jacobi-Anger series expansion, i.e.,

$$\mathsf{exp}\left\{\pm\zeta\sin(\omega t)\right\}=\sum_{m=-\infty}^{\infty}\mathcal{J}_m\left(\pm\zeta\right)\,\mathsf{e}^{im\omega t}\ , \tag{B11}$$

where $\mathcal{J}_m(\zeta)$ is the Bessel function of the first kind. We will also apply the orthogonality condition for the Fourier expansion function, namely,

$$\int_0^{T_0}dt\,\mathsf{e}^{in\omega t}\cdot\mathsf{e}^{-im\omega t}=\delta_{n,m}$$

for any fixed integer $-\infty<m<\infty$. As a result, we arrive at the following set of coupled linear algebraic equations, i.e.,

$$\begin{aligned}
&\left\{\mp k_x-\frac{\varepsilon_d(\boldsymbol{k}|\,\tau,\phi)}{\hbar v_F}+l\omega\right\}f_l^{(\mp1)}\mp\frac{ik_y}{\sqrt{2}}\sum_{m=-\infty}^{\infty}\left\{\sin(2\phi)\,f_{l-m}^{(0)}\,\mathcal{J}_m\left(\pm\lambda_0\right)+\sqrt{2}\tau\cos(2\phi)\,f_{l-m}^{(\pm1)}\mathcal{J}_m\left(\pm2\lambda_0\right)\right\}=0\ ,\\
&\left\{-\frac{\varepsilon_d(\boldsymbol{k}|\,\tau,\phi)}{\hbar v_F}+l\omega\right\}f_l^{(0)}+\frac{ik_y}{\sqrt{2}}\,\sin(2\phi)\sum_{m=-\infty}^{\infty}\sum_{\alpha=\pm1}\alpha\mathcal{J}_m\left(-\alpha\,\lambda_0\right)\,f_{l-m}^{(-\alpha)}=0\ .
\end{aligned} \tag{B12}$$

Furthermore, we notice that two terms in the front brackets of Eq. (B12) all reduce to $l\omega$ for $l\neq0$ since $\hbar\omega\gg\varepsilon_d(\boldsymbol{k}|\,\tau,\phi)$ and $\hbar v_Fk_{x,y}$ in the case of off-resonant interaction. Therefore, Eq. (B12) is simplified into

$$\begin{aligned}
&l\omega f_l^{(\mp1)}=\pm\frac{ik_y}{\sqrt{2}}\sum_{m=-\infty}^{\infty}\left\{\sin(2\phi)\,f_{l-m}^{(0)}\,\mathcal{J}_m\left(\pm\lambda_0\right)+\sqrt{2}\tau\cos(2\phi)\,f_{l-m}^{(\pm1)}\mathcal{J}_m\left(\pm2\lambda_0\right)\right\}\ ,\\
&l\omega f_l^{(0)}=-\frac{ik_y}{\sqrt{2}}\,\sin(2\phi)\sum_{m=-\infty}^{\infty}\sum_{\alpha=\pm1}\alpha\mathcal{J}_m\left(-\alpha\lambda_0\right)\,f_{l-m}^{(-\alpha)}\ .
\end{aligned} \tag{B13}$$

Equation (B13) cannot be satisfied unless all the expansion coefficients $f_l^{(0,\pm1)}=0$ for $l\neq0$. For this reason, we will just follow the standard procedure [17,34] by eliminating all the terms $f_l^{(0,\pm1)}$ for $l\neq0$. Once only the $l=0$ terms are retained in Eq. (B13), we simply get

$$\left\{\overleftrightarrow{\mathcal{K}}(\boldsymbol{k}|\,\tau,\phi)-\frac{\varepsilon_d(\boldsymbol{k}|\,\tau,\phi)}{\hbar v_F}\overleftrightarrow{\mathcal{I}}\right\}\otimes\begin{bmatrix} f_0^{(-1)}\\ f_0^{(0)}\\ f_0^{(1)}\end{bmatrix}=0\ , \tag{B14}$$

where $\overleftrightarrow{\mathcal{I}}$ is the unit matrix, and

$$\overleftrightarrow{\mathcal{K}}(\boldsymbol{k}|\,\tau,\phi)=\begin{bmatrix} -k_x/2 & -(ik_y/\sqrt{2})\sin(2\phi)\,\mathcal{J}_0(\lambda_0) & -i\tau k_y\cos(2\phi)\,\mathcal{J}_0(2\lambda_0)\\ 0 & 0 & -(ik_y/\sqrt{2})\sin(2\phi)\,\mathcal{J}_0(\lambda_0)\\ 0 & 0 & k_x/2\end{bmatrix}\ +\ h.c.\quad . \tag{B15}$$

Here, $h.c.$ means adding a Hermitian conjugate matrix, and we have also used the fact that $\mathcal{J}_0(\xi)=\mathcal{J}_0(-\xi)\backsimeq 1-\xi^2/4$ for $\xi=\lambda_0$ and $2\lambda_0$.

Finally, the eigenvalue equation in Eq. (B14) can be easily solved to give

$$\begin{aligned}&\varepsilon_d^{\gamma=0}(\boldsymbol{k}|\,\phi)=0\ ,\\ &\varepsilon_d^{\gamma=\pm1}(\boldsymbol{k}|\,\phi)=\pm\hbar v_F k\,f(\theta_{\mathbf{k}}|\,\phi)\ ,\end{aligned} \tag{B16}$$

which becomes independent of τ, where $f(\theta_{\mathbf{k}}|\,\phi)=\sqrt{\mathbb{A}(\theta_{\mathbf{k}}|\,\phi)}$, and the angular function is

$$\mathbb{A}(\theta|\,\phi)=\cos^2\theta+\left\{\left[\mathcal{J}_0(2\lambda_0)\cos(2\phi)\right]^2+\left[\mathcal{J}_0(\lambda_0)\sin(2\phi)\right]^2\right\}\sin^2\theta\ . \tag{B17}$$

Here, $\mathbb{A}(\theta|\,\phi)$ displays an anisotropy in the energy dispersions due to electron-photon interaction, which reduces to $\mathcal{J}_0^2(2\lambda_0)$ for graphene [34] with $\phi=0$. For a dice lattice with $\phi=\pi/4$, on the other hand, only the term $\mathcal{J}_0^2(\lambda_0)$ remains, which is found weaker than the electron-photon interaction in graphene.

For off-resonant radiation with low intensity, i.e., $\lambda_0=c_0/\hbar\omega\ll 1$, the conduction and valence bands energy dispersions are further approximated as

$$\varepsilon_d^{\gamma=\pm1}(\boldsymbol{k}|\,\phi)\backsimeq\gamma\hbar v_F\sqrt{k^2-\frac{\lambda_0^2}{4}\,\left[5+3\cos(4\phi)\right]\,k_y^2}\ . \tag{B18}$$

The anisotropy and difference between the Fermi velocities in the k_x and k_y directions for both valence and conduction bands reach the maximum for graphene with $\phi=0$ and the minimum for a dice lattice with $\phi=\pi/4$.

The corresponding wave function for the dressed-state quasiparticle, obtained from Eq. (B7), is

$$\begin{aligned}\Psi_d^{\gamma=\pm1}(\boldsymbol{k}|\,\tau,\phi)&=\frac{1}{\sqrt{\mathcal{N}_1(\boldsymbol{k}|\,\tau,\phi)}}\,\mathsf{e}^{\mp iv_F k f(\theta_{\mathbf{k}}|\,\phi)t}\\ &\times\left\{\frac{r_{11}(\boldsymbol{k}|\,\phi)}{\sqrt{2}}\begin{bmatrix}\tau\cos\phi\\ \pm1\\ \tau\sin\phi\end{bmatrix}\mathsf{e}^{\pm iz_\lambda(t)}+r_{12}(\boldsymbol{k}|\,\tau,\phi)\begin{bmatrix}\sin\phi\\ 0\\ -\cos\phi\end{bmatrix}+\frac{r_{13}(\boldsymbol{k}|\,\tau,\phi)}{\sqrt{2}}\begin{bmatrix}\tau\cos\phi\\ \mp1\\ \tau\sin\phi\end{bmatrix}\mathsf{e}^{\mp iz_\lambda(t)}\right\}\ ,\end{aligned} \tag{B19}$$

where

$$\begin{aligned}r_{11}(\boldsymbol{k}|\,\phi)&=2f(\theta_{\mathbf{k}}|\,\phi)\left[f(\theta_{\mathbf{k}}|\,\phi)+\cos\theta_{\mathbf{k}}\right]-\mathcal{J}_0^2(\lambda_0)\sin^2\theta_{\mathbf{k}}\sin^2(2\phi)\ ,\\ r_{12}(\boldsymbol{k}|\,\tau,\phi)&=-i\sqrt{2}\,\sin\theta_{\mathbf{k}}\sin(2\phi)\mathcal{J}_0(\lambda_0)\left[f(\theta_{\mathbf{k}}|\,\phi)+\cos\theta_{\mathbf{k}}+i\tau\sin\theta_{\mathbf{k}}\cos(2\phi)\mathcal{J}(2\lambda_0)\right]\ ,\\ r_{13}(\boldsymbol{k}|\,\tau,\phi)&=-\sin\theta_{\mathbf{k}}\left[\sin\theta_{\mathbf{k}}\sin^2(2\phi)\mathcal{J}_0^2(\lambda_0)+2i\tau f(\theta_{\mathbf{k}}|\,\phi)\cos(2\phi)\mathcal{J}_0(2\lambda_0)\right]\ ,\end{aligned} \tag{B20}$$

and the normalization factor is just $\mathcal{N}_1(\boldsymbol{k}|\,\tau,\phi)=\left|\Psi_d^{\gamma=\pm1}(\boldsymbol{k}|\,\tau,\phi)\right|^2$.

For the flat band with $\gamma = 0$, on the other hand, the wave function takes the form

$$\Psi_d^{\gamma=0}(\boldsymbol{k}|\,\tau,\phi) = \frac{1}{\sqrt{2\mathcal{N}_0(\boldsymbol{k}|\,\phi)}} \times \left\{ \frac{r_{01}(\boldsymbol{k}|\,\phi)\,\tau}{\sqrt{2}} \sum_{\alpha=\pm1} \mathsf{e}^{i\alpha z_\lambda(t)} \begin{bmatrix} \cos\phi \\ \alpha\tau \\ \sin\phi \end{bmatrix} + r_{02}(\boldsymbol{k}|\,\tau,\phi) \begin{bmatrix} \sin\phi \\ 0 \\ -\cos\phi \end{bmatrix} \right\} , \tag{B21}$$

where

$$\begin{aligned} r_{01}(\boldsymbol{k}|\,\phi) &= -i\sin(2\phi)\,\sin\theta_{\mathbf{k}}\,\mathcal{J}_0(\lambda_0)\ , \\ r_{02}(\boldsymbol{k}|\,\tau,\phi) &= \sqrt{2}\,[\cos\theta_{\mathbf{k}} + i\tau\cos(2\phi)\sin\theta_{\mathbf{k}}\,\mathcal{J}_0(2\lambda_0)]\ . \end{aligned} \tag{B22}$$

For the case of a dice lattice with $\phi = \pi/4$, we get from Eq. (B19) that

$$\begin{aligned} \Psi_d^{\gamma=\pm1}(\boldsymbol{k},t|\,\tau) = \mathsf{e}^{\mp iv_F k f_1(\theta_{\mathbf{k}})t}\,\frac{f_1(\theta_{\mathbf{k}})+\cos\theta_{\mathbf{k}}}{4f_1(\theta_{\mathbf{k}})} \Bigg\{ \mathsf{e}^{\pm iz_\lambda(t)} \begin{bmatrix} \tau \\ \pm\sqrt{2} \\ \tau \end{bmatrix} \\ -\frac{2i\mathcal{J}_0(\lambda_0)\sin\theta_{\mathbf{k}}}{f_1(\theta_{\mathbf{k}})+\cos\theta_{\mathbf{k}}} \begin{bmatrix} 1 \\ 0 \\ -1 \end{bmatrix} - \left(\frac{\mathcal{J}_0(\lambda_0)\sin\theta_{\mathbf{k}}}{f_1(\theta_{\mathbf{k}})+\cos\theta_{\mathbf{k}}}\right)^2 \begin{bmatrix} \tau \\ \mp\sqrt{2} \\ \tau \end{bmatrix} \mathsf{e}^{\mp iz_\lambda(t)} \Bigg\} , \end{aligned} \tag{B23}$$

where

$$f_1(\theta_{\mathbf{k}}) = f(\theta_{\mathbf{k}}|\,\phi=\pi/4) = \sqrt{\cos^2\theta_{\mathbf{k}} + \sin^2\theta_{\mathbf{k}}\,\mathcal{J}_0^2(\lambda_0)} \tag{B24}$$

and $z_\lambda(t) = \lambda_0\sin(\omega t)$. The wave function in Eq. (B23) at $t = 0$ could be presented in a simplified way, yielding

$$\Psi_d^{\gamma=\pm1}(\boldsymbol{k}|\,\tau) = \frac{1}{2} \begin{bmatrix} \tau\mathsf{e}^{-i\Phi_1(\theta_{\mathbf{k}}|\,\tau)} \\ \gamma\sqrt{2} \\ \tau\mathsf{e}^{i\Phi_1(\theta_{\mathbf{k}}|\,\tau)} \end{bmatrix} , \tag{B25}$$

$$\Phi_1(\theta_{\mathbf{k}}|\,\tau) = 2\arctan\left\{\frac{\tau\mathcal{J}_0(\lambda_0)\sin\theta_{\mathbf{k}}}{f_1(\theta_{\mathbf{k}})+\cos\theta_{\mathbf{k}}}\right\} \backsimeq \tau\left\{\theta_{\mathbf{k}} - \frac{\lambda_0^2}{8}\,\sin^2(2\theta_{\mathbf{k}}) + \cdots\right\} .$$

where the phase $\Phi_1(\theta_{\mathbf{k}}|\,\tau)$ for dice lattices differs from that in graphene by the correction from the weak-coupling constant $\lambda_0 \ll 1$.

The remaining wave function for the flat band with $\gamma = 0$ takes the form

$$\Psi_d^{\gamma=0}(\boldsymbol{k},t|\,\tau) = \frac{1}{\sqrt{2}f_1(\theta_{\mathbf{k}})} \left\{ -\frac{i\tau}{2}\,\sin\theta_{\mathbf{k}}\,\mathcal{J}_0(\lambda_0) \sum_{\alpha=\pm1} \mathsf{e}^{i\alpha z_\lambda(t)} \begin{bmatrix} 1 \\ \sqrt{2}\alpha\tau \\ 1 \end{bmatrix} + \cos\theta_{\mathbf{k}} \begin{bmatrix} 1 \\ 0 \\ -1 \end{bmatrix} \right\} . \tag{B26}$$

The structure of the wave function in Eq. (B26) is such that at $t = 0$ it consists of two components of equal amplitudes and phase difference $\Phi_0(\theta_{\mathbf{k}}|\,\tau)$, and could be rewritten as

$$\Psi_d^{\gamma=0}(\boldsymbol{k}|\,\tau) = \frac{1}{\sqrt{2}} \begin{bmatrix} \mathsf{e}^{-i\Phi_0(\theta_{\mathbf{k}}|\,\tau)} \\ 0 \\ -\mathsf{e}^{i\Phi_0(\theta_{\mathbf{k}}|\,\tau)} \end{bmatrix} , \tag{B27}$$

$$\Phi_0(\theta_{\mathbf{k}}|\,\tau) = \arctan\left\{\tau\mathcal{J}_0(\lambda_0)\tan\theta_{\mathbf{k}}\right\} \backsimeq \tau\left\{\theta_{\mathbf{k}} - \frac{\lambda_0^2}{2}\sin(2\theta_{\mathbf{k}}) + \cdots\right\} .$$

Appendix C: Dressing field-induced modifications to Berry phases

In this part, we provide details of the *Berry phase* evaluation for the dressed-state wave functions in Eqs. (19) and (21) with a circularly polarized field applied to a dice lattice, as well as for the eigenstates in Eqs. (29)-(32) and in Eqs. (36) and (37), corresponding to various types of α-T_3 lattices interacting with a linearly polarized field. We also explain the derivation of the Berry connection and curvature.

By using polar coordinates, the general expression for gradient $\boldsymbol{\nabla}_{\mathbf{k}}$ and the vector length element $d\boldsymbol{k}$ can be expressed as [63]

$$\begin{aligned} \boldsymbol{\nabla}_{\mathbf{k}} &= \frac{\partial}{\partial k}\,\hat{\boldsymbol{e}}_{\mathbf{k}} + \frac{1}{k}\frac{\partial}{\partial \theta_{\mathbf{k}}}\,\hat{\boldsymbol{e}}_{\theta}\ , \\ d\boldsymbol{k} &= dk\,\hat{\boldsymbol{e}}_{\mathbf{k}} + k\,d\theta_{\mathbf{k}}\,\hat{\boldsymbol{e}}_{\theta}\ . \end{aligned} \tag{C1}$$

As a first step, we must choose the proper *closed integration path* for Eq. (41). In order to satisfy the requirement of an adiabatic (or isoenergetic) evolution of a quantum system, during which a Berry phase is accumulated, we have to choose a path with a constant energy of our quasiparticle, i.e., with a constraint of $\varepsilon_d^{\gamma=\pm 1}(\boldsymbol{k}|\,\tau,\phi) = \varepsilon_0 = \text{const}$.

For the first case of a dice lattice interacting with circularly polarized light, the energy dispersions in Eq. (18) and the corresponding eigenstates in Eqs. (19) and (21) are isotropic in $\boldsymbol{k}$ space, so that the required path can be chosen as *a circle of radius* k_0. While the wave function components and their scalar product in this case still depend on k and $\theta_{\mathbf{k}}$, the integration variable in Eq. (41) is simply written as $d\boldsymbol{k} = k_0\,d\theta_{\mathbf{k}}\,\hat{\boldsymbol{e}}_{\theta}$. We begin with the eigenstates in Eq. (19) associated with valence and conduction bands. For any circular path of radius k_0, the Berry phase defined in Eq. (41) is calculated as

$$\Phi_B^{(c)}(\gamma,k_0|\,\tau=1) = \frac{\mathcal{C}_1^2(\gamma,k_0)-1}{\mathcal{N}(\gamma,k_0)}\int\limits_0^{2\pi} d\theta_{\mathbf{k}} \backsimeq \pi\gamma\,\frac{c_0}{\hbar v_F k_0}\,\lambda_0\ . \tag{C2}$$

In addition, we have $\Phi_B^{(c)}(\gamma,k_0|\,\tau=-1) = -\Phi_B^{(c)}(\gamma,k_0|\,\tau=1)$ for the K' valley, similar to the case of a non-irradiated α-T_3 lattice. In the absence of the circularly polarized irradiation, however, the Berry phase for a dice lattice is zero due to the fact [56] that $\Phi_B^{(0)}(\gamma,k_0|\,\tau) = \tau\pi\cos(\pi/2) = 0$. Furthermore, the Berry phase of the flat band remains zero in the presence of circularly polarized light, which could be easily verified by evaluating the integral in Eq. (41) with respect to the wave function in Eq. (21).

In contrast, for α-T_3 lattices the constant-energy cut of dispersions in Eq. (26) with angular dependence given by Eq. (27) has an elliptic shape, as displayed in Fig. 4(a). Such an ellipse is described by

$$\left[\frac{k_1(\theta_{\mathbf{k}})\cos(\theta_{\mathbf{k}})}{a}\right]^2 + \left[\frac{k_1(\theta_{\mathbf{k}})\sin(\theta_{\mathbf{k}})}{b(\phi)}\right]^2 = 1\,, \tag{C3}$$

where

$$\begin{aligned} a &= \frac{\varepsilon_0}{\hbar v_F}\,, \\ b(\phi) &= \frac{\varepsilon_0}{\hbar v_F}\,\left\{\left[\mathcal{J}_0(2\lambda_0)\cos(2\phi)\right]^2 + \left[\mathcal{J}_0(\lambda_0)\sin(2\phi)\right]^2\right\}^{-1} \backsimeq a\,\left\{1+\frac{\lambda_0^2}{8}\,\left[5+3\cos(4\phi)\right]\right\} > a\ . \end{aligned} \tag{C4}$$

Moreover, we have defined

$$k_1(\theta_{\mathbf{k}}) = \frac{b(\phi)\,a}{\sqrt{a^2\cos^2\theta_{\mathbf{k}} + b^2(\phi)\sin^2\theta_{\mathbf{k}}}} = \frac{b(\phi)}{\sqrt{1-e^2(\phi)\cos^2\theta_{\mathbf{k}}}}\ , \tag{C5}$$

where a and $b(\phi)$ are major and minor semi-axes of an ellipse in $\boldsymbol{k}$ space and $e(\phi) = \sqrt{1-b^2(\phi)/a^2}$ is its *eccentricity*. We see that each specific elliptical path, as well as its eccentricity, also depends on the intensity of incoming radiation or

coupling constant λ_0. Our notation $\theta_{\mathbf{k}} = \arctan(k_y/k_x)$ should not lead to confusion since the angle $\theta_{\mathbf{k}}$ is independent of the radial component k in polar coordinates. For the current case, we find

$$dk_1(\theta_{\mathbf{k}}) = -\frac{1}{2}\, b(\phi)\, e^2(\phi)\, \frac{\sin(2\theta_{\mathbf{k}})}{[1-e^2(\phi)\cos\theta_{\mathbf{k}}]^{2/3}}\, d\theta_{\mathbf{k}} \ , \tag{C6}$$

$$d\boldsymbol{k} = \frac{b(\phi)}{\sqrt{1-e^2(\phi)\cos\theta_{\mathbf{k}}}} \left\{ \hat{\boldsymbol{e}}_\theta - \frac{e^2(\phi)\sin(2\theta_{\mathbf{k}})}{2\,[1-e^2(\phi)\cos\theta_{\mathbf{k}}]}\, \hat{\boldsymbol{e}}_{\mathbf{k}} \right\} d\theta_{\mathbf{k}} \ . \tag{C7}$$

Particularly, in the case of linearly polarized light, we notice that the wave function components in Eqs. (31) and (33) depend only on $\theta_{\mathbf{k}}$ but not on the radial component k for all possible values of ϕ. Therefore, we find from Eq. (31) that

$$\boldsymbol{\nabla}_{\mathbf{k}} \Psi_d^{\gamma=\pm1}(\boldsymbol{k}|\,\tau) = \frac{1}{k_1(\theta_{\mathbf{k}})}\, \frac{\partial}{\partial\theta_{\mathbf{k}}}\, \Psi_d^{\gamma=\pm1}(\boldsymbol{k}|\,\tau) = \frac{i\tau}{2k_1(\theta_{\mathbf{k}})}\, \frac{\partial\Phi_{0,1}(\theta_{\mathbf{k}}|\,\tau)}{\partial\theta_{\mathbf{k}}} \begin{bmatrix} -\mathsf{e}^{-i\Phi_{0,1}(\theta_{\mathbf{k}}|\,\tau)} \\ 0 \\ \mathsf{e}^{i\Phi_{0,1}(\theta_{\mathbf{k}}|\,\tau)} \end{bmatrix} \ , \tag{C8}$$

so that $\left[\Psi_d^{\gamma=\pm1}(\boldsymbol{k}|\,\tau)\right]^\dagger \boldsymbol{\nabla}_{\mathbf{k}} \Psi_d^{\gamma=\pm1}(\boldsymbol{k}|\,\tau) \equiv 0$. The only difference between the flat and the valence/conduction bands is the explicit expressions for $\Phi_0(\theta_{\mathbf{k}}|\,\tau)$ and $\Phi_1(\theta_{\mathbf{k}}|\,\tau)$, which will not change the fact of a zero Berry phase from Eq. (41).

In the remaining part of Appendix C, we would like to show details of the calculation on the Berry connection vector field $\mathbf{A}^{\gamma}_{\tau,\phi}(\mathbf{k},\lambda_0)$ and the Berry curvature $\boldsymbol{\Omega}^{\gamma}_{\tau,\phi}(\mathbf{k},\lambda_0)$, which are defined by

$$\begin{aligned} &\mathbf{A}^{\gamma}_{\tau,\phi}(\mathbf{k},\lambda_0) \equiv \langle \Psi_d^{\gamma}(\mathbf{k},\lambda_0|\,\tau,\phi)|\, i\boldsymbol{\nabla}_{\mathbf{k}}\, |\Psi_d^{\gamma}(\mathbf{k},\lambda_0|\,\tau,\phi)\rangle \ , \\ &\boldsymbol{\Omega}^{\gamma}_{\tau,\phi}(\mathbf{k},\lambda_0) \equiv \boldsymbol{\nabla}_{\mathbf{k}} \times \mathbf{A}^{\gamma}_{\tau,\phi}(\mathbf{k},\lambda_0) \ . \end{aligned} \tag{C9}$$

In the absence of incident light, the Berry connections for the cone bands with $\gamma = \pm1$ are $\mathbf{A}^{\gamma=\pm1}_{\tau,\phi}(\mathbf{k},\lambda_0) = +(\tau/2)\cos(2\phi)\,\boldsymbol{\nabla}_{\mathbf{k}}\theta_{\mathbf{k}}$ and $\mathbf{A}^{\gamma=0}_{\tau,\phi}(\mathbf{k},\lambda_0) = -2\mathbf{A}^{\gamma=\pm1}_{\tau,\phi}(\mathbf{k},\lambda_0)$ for the flat band. The $\times2$ difference comes from the normalization of different wave functions.

In polar coordinates, according to Eq. (C1), $\boldsymbol{\nabla}_{\mathbf{k}}\theta_{\mathbf{k}} = (1/k)\,\hat{e}_\theta$ is directed along the $\hat{e}_\theta$ unit vector. We immediately find that for all bands ($\gamma = 0, \pm1$) the Berry field is always zero for a dice lattice with $\phi = \pi/4$.

It is straightforward to verify that for a dice lattice the Berry connection *will remain zero even in the presence of a linearly polarized dressing field.* As described above, for a dice lattice with $\alpha = 1$, we get $\left[\Psi_d^{\gamma=\pm1}(\boldsymbol{k}|\,\tau)\right]^\dagger \boldsymbol{\nabla}_{\mathbf{k}} \Psi_d^{\gamma=\pm1}(\boldsymbol{k}|\,\tau) \equiv 0$. Here, the only difference between the flat and valence/conduction bands is the explicit expressions of phases $\Phi_0(\theta_{\mathbf{k}}|\,\tau)$ for $\gamma = 0$ and $\Phi_1(\theta_{\mathbf{k}}|\,\tau)$ for $\gamma = \pm1$. We would also like to emphasize that the Berry connection is closely connected to the Berry phase defined in Eq. (41), except that the closed-linear integration is not performed.

Furthermore, the Berry curvature is calculated as

$$\hat{e}_z \cdot \left[\boldsymbol{\nabla}_{\mathbf{k}} \times \mathbf{A}^{\gamma}_{\tau,\phi}(\mathbf{k},\lambda_0)\right] = \frac{1}{k}\left(\frac{\partial[k(A^{\gamma}_{-,\phi})_\theta]}{\partial k} - \frac{\partial(A^{\gamma}_{-,\phi})_k}{\partial\theta_{\mathbf{k}}}\right) = \frac{\tau}{2k}\,\cos(2\phi)\frac{d}{dk}\,\Theta(k) \ , \tag{C10}$$

where $\Theta(k)$ is a step function which is introduced because k/k is always 1 if k is finite but undetermined for $k = 0$. Here, we also make use of the following identity in the polar coordinates, i.e., $\delta(\mathbf{k}) = \delta(k)/(2\pi k)$, where $\delta(k) = d\Theta(k)/dk$ is the Dirac delta function. Finally, from Eq. (C10) we obtain

$$\begin{aligned} &\boldsymbol{\Omega}^{\gamma=\pm1}_{\tau,\phi}(\mathbf{k},\lambda_0=0) = \tau\pi\,\cos(2\phi)\,\delta(\mathbf{k}) \ , \\ &\boldsymbol{\Omega}^{\gamma=0}_{\tau,\phi}(\mathbf{k},\lambda_0=0) = -2\tau\pi\,\cos(2\phi)\,\delta(\mathbf{k}) \ . \end{aligned} \tag{C11}$$

These results imply a complete valley symmetry since each of them is proportional to the valley-index τ.

---

[1] J. D. Malcolm and E. J. Nicol, Physical Review B **93**, 165433 (2016).
[2] B. Dey and T. K. Ghosh, Physical Review B **98**, 075422 (2018).
[3] K. Novoselov, A. K. Geim, S. Morozov, D. Jiang, M. Katsnelson, I. Grigorieva, S. Dubonos, and A. Firsov, nature **438**, 197 (2005).
[4] R. R. Nair, P. Blake, A. N. Grigorenko, K. S. Novoselov, T. J. Booth, T. Stauber, N. M. Peres, and A. K. Geim, Science **320**, 1308 (2008).
[5] A. C. Ferrari, J. Meyer, V. Scardaci, C. Casiraghi, M. Lazzeri, F. Mauri, S. Piscanec, D. Jiang, K. Novoselov, S. Roth, et al., Physical review letters **97**, 187401 (2006).
[6] M. Rizzi, V. Cataudella, and R. Fazio, Physical Review B **73**, 144511 (2006).
[7] J. Vidal, R. Mosseri, and B. Douçot, Physical review letters **81**, 5888 (1998).
[8] N. Goldman and J. Dalibard, Physical review X **4**, 031027 (2014).
[9] P. Perez-Piskunow, G. Usaj, C. Balseiro, and L. F. Torres, Physical Review B **89**, 121401 (2014).
[10] E. S. Morell and L. E. F. Torres, Physical Review B **86**, 125449 (2012).
[11] Z. Gu, H. Fertig, D. P. Arovas, and A. Auerbach, Physical review letters **107**, 216601 (2011).
[12] V. Kozin, I. Iorsh, O. Kibis, and I. Shelykh, Physical Review B **97**, 035416 (2018).
[13] S. Mandal, T. Liew, and O. Kibis, Physical Review A **97**, 043860 (2018).
[14] S. Morina, O. V. Kibis, A. A. Pervishko, and I. A. Shelykh, Phys. Rev. B **91**, 155312 (2015).
[15] O. Kibis, Physical Review B **81**, 165433 (2010).
[16] O. Kibis, K. Dini, I. Iorsh, and I. Shelykh, Physical Review B **95**, 125401 (2017).
[17] A. Iurov, L. Zhemchuzhna, G. Gumbs, and D. Huang, Journal of Applied Physics **122**, 124301 (2017).
[18] O. Kibis, K. Dini, I. Iorsh, and I. Shelykh, Semiconductors **52**, 523 (2018).
[19] T. Oka and H. Aoki, Physical Review B **79**, 081406 (2009).
[20] B. Dóra, J. Cayssol, F. Simon, and R. Moessner, Physical review letters **108**, 056602 (2012).
[21] D. Abergel and T. Chakraborty, Applied Physics Letters **95**, 062107 (2009).
[22] H. L. Calvo, J. S. Luna, V. Dal Lago, and L. E. F. Torres, Physical Review B **98**, 035423 (2018).
[23] V. Dal Lago, E. S. Morell, and L. F. Torres, Physical Review B **96**, 235409 (2017).
[24] G. Usaj, P. Perez-Piskunow, L. F. Torres, and C. Balseiro, Physical Review B **90**, 115423 (2014).
[25] A. Iurov, G. Gumbs, O. Roslyak, and D. Huang, Journal of Physics: Condensed Matter **25**, 135502 (2013).
[26] D. Yudin, O. Kibis, and I. Shelykh, New Journal of Physics **18**, 103014 (2016).
[27] I. Iorsh, K. Dini, O. Kibis, and I. Shelykh, Physical Review B **96**, 155432 (2017).
[28] M. Katsnelson, K. Novoselov, and A. Geim, Nature physics **2**, 620 (2006).
[29] H. L. Calvo, H. M. Pastawski, S. Roche, and L. E. F. Torres, Applied Physics Letters **98**, 232103 (2011).
[30] A. Iurov, G. Gumbs, O. Roslyak, and D. Huang, Journal of Physics: Condensed Matter **24**, 015303 (2011).
[31] G. Gumbs, A. Iurov, D. Huang, P. Fekete, and L. Zhemchuzhna, in *AIP Conference Proceedings* (AIP, 2014), vol. 1590, pp. 134–142.
[32] S. Morina, K. Dini, I. V. Iorsh, and I. A. Shelykh, ACS Photonics **5**, 1171 (2018).
[33] A. Iurov, G. Gumbs, and D. Huang, Journal of Modern Optics **64**, 913 (2017).
[34] K. Kristinsson, O. Kibis, S. Morina, and I. Shelykh, Scientific reports **6**, 20082 (2016).
[35] Z. Li, T. Cao, M. Wu, and S. G. Louie, Nano letters **17**, 2280 (2017).
[36] E. Illes and E. Nicol, Physical Review B **95**, 235432 (2017).
[37] D. F. Urban, D. Bercioux, M. Wimmer, and W. Häusler, Physical Review B **84**, 115136 (2011).
[38] E. Illes, J. Carbotte, and E. Nicol, Physical Review B **92**, 245410 (2015).
[39] A. Raoux, M. Morigi, J.-N. Fuchs, F. Piéchon, and G. Montambaux, Physical review letters **112**, 026402 (2014).
[40] F. Piéchon, J. Fuchs, A. Raoux, and G. Montambaux, in *Journal of Physics: Conference Series* (IOP Publishing, 2015), vol. 603, p. 012001.
[41] E. Illes and E. Nicol, Physical Review B **94**, 125435 (2016).
[42] T. Biswas and T. K. Ghosh, Journal of Physics: Condensed Matter **28**, 495302 (2016).
[43] T. Biswas and T. K. Ghosh, Journal of Physics: Condensed Matter **30**, 075301 (2018).
[44] M. Gyamfi, T. Eelbo, M. Waśniowska, T. O. Wehling, S. Forti, U. Starke, A. I. Lichtenstein, M. I. Katsnelson, and R. Wiesendanger, Phys. Rev. B **85**, 161406 (2012).
[45] J.-K. Lee, S.-C. Lee, J.-P. Ahn, S.-C. Kim, J. I. Wilson, and P. John, The Journal of chemical physics **129**, 234709 (2008).
[46] O. Vilkov, A. Fedorov, D. Usachov, L. Yashina, A. Generalov, K. Borygina, N. Verbitskiy, A. Grüneis, and D. Vyalikh, Scientific reports **3**, 2168 (2013).
[47] F. Mahmood, C.-K. Chan, Z. Alpichshev, D. Gardner, Y. Lee, P. A. Lee, and N. Gedik, Nature Physics **12**, 306 (2016).
[48] N. Fläschner, B. Rem, M. Tarnowski, D. Vogel, D.-S. Lühmann, K. Sengstock, and C. Weitenberg, Science **352**, 1091 (2016).
[49] C. J. Tabert and E. J. Nicol, Physical Review B **89**, 195410 (2014).
[50] M. Ezawa, New Journal of Physics **14**, 033003 (2012).
[51] A. Iurov, G. Gumbs, and D. Huang, Physical Review B **98**, 075414 (2018).

[52] H.-Y. Xu, L. Huang, D. Huang, and Y.-C. Lai, Physical Review B **96**, 045412 (2017).
[53] O. L. Berman, Y. E. Lozovik, and G. Gumbs, Physical Review B **77**, 155433 (2008).
[54] M. V. Berry, Proc. R. Soc. Lond. A **392**, 45 (1984).
[55] D. Xiao, M.-C. Chang, and Q. Niu, Reviews of modern physics **82**, 1959 (2010).
[56] E. Illes, Ph.D. thesis (2017), URL `http://atrium.lib.uoguelph.ca/xmlui/handle/10214/11512`.
[57] T. Louvet, P. Delplace, A. A. Fedorenko, and D. Carpentier, Physical Review B **92**, 155116 (2015).
[58] Y. Aharonov and D. Bohm, Physical Review **115**, 485 (1959).
[59] L. Lu, J. D. Joannopoulos, and M. Soljačić, Nature Photonics **8**, 821 (2014).
[60] M. J. Ablowitz and J. T. Cole, Physical Review A **99**, 033821 (2019).
[61] B. Dey and T. K. Ghosh, arXiv preprint arXiv:1901.10778 (2019).
[62] F. Zhang, A. H. MacDonald, and E. J. Mele, Proceedings of the National Academy of Sciences **110**, 10546 (2013).
[63] G. B. Arfken and H. J. Weber, *Mathematical methods for physicists* (1999).
[64] The actual irradiation frequencies, suggested for the experimental verification of our results depend on the initial bandgap of the material considered. Specifically, since non-irradiated α-T_3 does not acquires an energy gap between the valence, conduction and flat bands, our predicted features could be verified in the THz frequency range.